Bioactive isoprenoids guide migrating germ cells to the embryonic gonad

Barton, Lacy J[1], Sanny, Justina[1], Dawson, Emily P[1], Nouzova, Marcela[2,3], Noriega, Fernando Gabriel[2], Stadtfeld, Matthias[1,4], Lehmann, Ruth[1,5]

[1] Department of Cell Biology, Skirball Institute of Biomolecular Medicine, NYU Grossman School of Medicine, NY, USA, 540 First Avenue, New York, NY 10016

[2] Department of Biological Sciences and Biomolecular Sciences Institute, Florida International University, 11200 SW 8th St, Miami, FL 33199

[3] Institute of Parasitology, Biology Centre CAS, Ceske Budejovice, Czech Republic

[4] Present: Department of Medicine, Weill Cornell Medicine, 413 E 69th St, New York, NY 10021

[5] Present: Department of Biology, Whitehead Institute Biology at MIT, 455 Mainstreet, Cambridge, MA 02142

Abstract

Germ cells are essential to sexual reproduction. Across the animal kingdom, extracellular isoprenoids, such as retinoic acids (RAs) in vertebrates and juvenile hormones (JHs) in insects, impact the germline lifecycle from meiosis to gametogenesis. Emerging evidence suggests that these bioactive isoprenoids broadly influence embryonic reproductive development, though the precise functions remain unclear. Here, we investigated the role of bioactive isoprenoids in early germ cell development using JHs in *Drosophila* as a model. With a newly generated *in vivo* reporter, we find that JH signaling is active in the vicinity of germ cells as they migrate to colonize the somatic gonad. Through a combination of *in vivo* and *in vitro* assays, we find that JHs are both necessary and sufficient for primordial germ cell migration through mechanisms independent of canonical nuclear receptor-mediated transcription. These findings reveal that JH is present during *Drosophila* embryogenesis and that bioactive isoprenoids impact germ cell development earlier than previously appreciated. Interestingly, we find that like JH in *Drosophila*, RA is sufficient for murine germ cell migration *in vitro*, suggesting that the impact of bioactive isoprenoids on embryonic germ cell development may be broadly conserved.

35 **Main**

36

37 Animal reproduction requires the precise specification, development, and protection of germ
38 cells. In many species, a critical stage in germ cell development occurs within a narrow window
39 of embryogenesis, during which primordial germ cells (PGCs) migrate long distances to colonize
40 the developing somatic gonad[1], often while undergoing genome-wide epigenetic and
41 transcriptional changes[2, 3] and overcoming selective survival barriers[4]. Shortly after colonizing
42 the somatic gonad, PGCs commit to gametogenesis[5], and together with somatic gonadal cells,
43 undergo sex-specific differentiation. Failure to complete these processes causes diverse
44 complications ranging from extragonadal germ cell tumors to infertility. Despite these important
45 consequences, how PGCs complete and coordinate these temporally overlapping processes
46 during early embryogenesis remains enigmatic and an active area of investigation.

47

48 Germ cell development is regulated by signals coming from the extracellular environment. One
49 family of extracellular factors are isoprenoid lipids. These bioactive lipids are found across the
50 animal kingdom, including retinoic acids (RAs) in vertebrates, methyl farnesoate in crustaceans
51 and some insects, and juvenile hormones (JHs) in insects. In many species, isoprenoids are
52 produced in and near the somatic gonad and exert powerful effects on reproduction. In
53 crustaceans, isoprenoids are both necessary and sufficient for sex determination[6]. In mice, RAs
54 have long been implicated as a meiosis-inducing factor, with the male-specific delay in meiotic
55 entry coinciding with male-specific expression of the gene encoding the RA degradation
56 enzyme, CYP26B1, in the somatic gonad [7, 8]. However, emerging evidence suggests that the
57 impact of RA on embryonic germ cell development is multifaceted and extends beyond meiosis[9,
58 10]. The most recent studies of RAs demonstrate that the precise roles for secreted isoprenoids
59 in embryonic reproductive development remains unclear[11-15].

60

61 Like RA in vertebrates, JHs impact multiple processes in the germline lifecycle. In fact, JHs are
62 the central gonadotropic hormones in many insects, regulating late stage gametogenesis and
63 reproductive diapause in adults[16]. Embryonic germ cell development in mice and *Drosophila*
64 have striking similarities in expression of isoprenoid enzymes. Like *CYP26B1* in mice,
65 expression of the gene encoding JH degradation enzyme, JH epoxide hydrolase 2 (Jheh2), is
66 induced in the embryonic male gonad[17]. Expression of isoprenoid biosynthetic enzymes also
67 overlap. In mice, genes encoding key RA enzymes, *Retinaldehyde dehydrogenases*
68 (*RALDH*)*1,2, and 3*, are expressed in and near the genital ridge as primordial germ cells (PGCs)

colonize the mesodermal gonad[13, 18]. In *Drosophila*, the key JH biosynthetic enzyme, JH acid methyltransferase (Jhamt), is expressed in the mesoderm during the same corresponding window of germ cell development in embryogenesis[19]. Yet, despite these striking similarities, whether JHs regulate PGC development is unknown.

Here we investigated the role of JHs in early *Drosophila* germ cell development. To determine whether mesodermal *jhamt* expression drives JH biosynthesis, we generated an *in vivo* JH reporter, finding that JH signaling is first active near PGCs as they migrate towards the developing somatic gonadal precursors. Using newly generated *jhmat* mutants, the first germline phenotype we observe is an increase in extragonadal PGCs after migration to the gonad is complete. Strikingly, this phenotype is shared with mutations in the rate-limiting enzyme of the mevalonate pathway upstream of JH biosynthesis, HMG Coenzyme A reductase (Hmgcr), an enzyme that is both necessary and sufficient for PGC migration in *Drosophila*[20]. With a combination of *in vivo* and *in vitro* assays, we find JHs are sufficient for PGC migration. We provide evidence that the effect of JH on germ cell migration is independent of canonical transcription-dependent signaling, but instead involves the cytoplasmic calcium signaling factor, Phospholipase C at 21c (Plc21c). Together, these data reveal a new requirement for secreted isoprenoids in early germ cell development. Finally, we find that the vertebrate isoprenoid, RA, is sufficient to induce migration of both *Drosophila* and mouse embryonic germ cells, suggesting this newly identified role of isoprenoids on early germ cell development may be broadly shared across invertebrate and vertebrate species.

Results

Juvenile hormone signaling is active during early germ cell development in *Drosophila* embryos

Isoprenoid bioavailability is governed by dynamic spatiotemporal expression of biosynthetic and degradation enzymes. Consistently, the key JH biosynthetic enzyme, Jhamt, is highly expressed in the endocrine gland called the *corpus allatum*, which is the major source of JH in larval and adult insects[21]. However, *Drosophila* embryos also express *jhamt*[19], though no function for JH in embryogenesis has been described. Given the important roles of isoprenoids in germline development and fertility, we determined where *jhamt* is expressed relative to germ cell development using dual-label fluorescent *in situ* hybridization for mRNAs encoding Jhamt and the germ cell factor, Nanos. Consistent with previous work[19], we found *jhamt* expression is enriched in the somatic mesoderm starting at embryonic Stage 10 (~4 hours after fertilization), continuing through Stage 13 (~11 hours after fertilization) (**Fig 1a and b**). This analysis revealed *jhamt* expression in proximity to PGCs as they enter and migrate within the mesoderm to colonize the developing somatic gonad (**Fig 1b**).

Mesodermal *jhamt* expression occurs prior to development of the *corpus allatum*[22] and thus whether mesodermal *jhamt* leads to *bona fide* JH production during *Drosophila* mid-embryogenesis was unknown. To detect JH signaling during embryogenesis, we generated an *in vivo eGFP* JH reporter by placing eight tandem copies of a JH response element (JHRE) from the *early trypsin* gene of *Aedes aegypti*[23, 24], which has been previously shown to robustly and specifically responds to JH *in vitro*[23]. To establish JH dependency *in vivo*, we fed second instar larvae the JH analogue, methoprene, and measured *GFP* mRNA by RT-qPCR. *GFP* transcription was induced more than 4-fold in *JHRE-GFP* larvae fed methoprene (**Fig 1c**). Expression of GFP did not increase in methoprene fed JHRE-GFP larvae lacking both JH nuclear receptors (JHNRs), Methoprene tolerant (Met) and Germ cell expressed (Gce) (**Fig 1c** and **Supp Fig 1b**). These data demonstrate that this fluorescent reporter faithfully responds to JH dynamics *in vivo*.

To determine whether JH is present and signaling is active during embryonic germ cell development, we stained *JHRE-GFP* embryos for GFP and the germ cell-specific RNA helicase, Vasa. GFP signal was first detected in Stage 10 embryos in two locations: in bilateral groups within the anterior head region and in the posterior germband (**Fig 1d**). Unlike the GFP signal in

137 the anterior region, signal in the posterior region was not detected in embryos carrying a
138 negative control reporter transgene, in which the Met/Gce binding motif of the JH response
139 element was mutated. Further investigation revealed that the GFP signal in the anterior region
140 was non-specific and localizes to hemocytes (**Supp Fig 1a-c**)[23]. Analysis of specific reporter
141 activity in the posterior germband revealed that JH signaling begins within the mesoderm at
142 Stage 10, when PGCs have migrated from the endoderm into the mesoderm, and continues to
143 localize near PGCs as they colonize the gonad (**Fig 1e, Supp 1c**). Together, these observations
144 demonstrate that JH activity is first detected in mid-embryogenesis in *Drosophila* prior to *corpus*
145 *allatum* development and is enriched in the mesoderm near PGCs that are migrating toward the
146 developing somatic gonadal precursors.
147
148
149 Juvenile hormones are required for migrating germ cells to reach the somatic gonad
150
151 The proximity of JH activity to the migrating and developing PGCs suggested a previously
152 unanticipated role for JH during *Drosophila* embryogenesis. To determine whether JH facilitates
153 germ cell development, we generated new mutant *jhamt* alleles by CRISPR gene editing in
154 which small, internal deletions induced frame-shifts at the start of the methyltransferase domain
155 critical for *jhamt* function (**Fig 2b**). In total, fifteen *jhamt* alleles were generated, two carrying a
156 stop codon at amino acid 46, while the remaining thirteen carry a stop codon at amino acid 54
157 (**Supp Fig 2a**). To avoid confounding effects from second site mutations, all analyses carried
158 out using the newly generated *jhamt* lines were performed in heteroallelic combinations or *in*
159 *trans* to a small deficiency lacking the entire *jhamt* locus. To verify loss of *jhamt* function, titers
160 of two major JH species in *Drosophila*, JH III and JHB_3, were determined by liquid
161 chromatography-tandem mass spectrometry[25]. As expected[26], animals with stop codon mutation
162 at the beginning of the methyltransferase domain have reduced JH III titers, undetectable JHB_3
163 titers (**Fig 2c**), and compromised female fecundity (**Fig 2d**).
164
165 To analyze germ cell development, wild type and *jhamt* mutant embryos from all stages of
166 embryogenesis were stained for Vasa and DAPI. This analysis revealed that the first detectable
167 germ cell defect in embryos zygotically mutant for *jhamt* was an increased number of germ cells
168 remaining outside the gonad after Stage 14, when PGC colonization of the somatic gonad is
169 complete (**Fig 2e,f**). Quantification of extragonadal PGCs revealed a significant increase in
170 *jhamt* mutant animals, but not when a complementing, $jhamt^+$ transgene gene was also

171 expressed in somatic cells (**Fig 2e,f**). These data indicate Jhamt facilitates PGC migration to the
172 developing somatic gonad.
173
174 Germ cells in *jhamt* mutant embryos exit the endoderm but remain posterior to the gonad, a
175 PGC migration phenotype similar to embryos lacking the key mevalonate pathway enzyme,
176 Hmgcr (**Fig 2e** and **f**)[20]. Hmgcr is both necessary and sufficient for PGC migration in *Drosophila*
177 such that ectopic expression of Hmgcr mislocalizes PGCs to a variety of locations[20, 27]. In larval
178 development, Jhamt functions downstream of Hmgcr in the biosynthesis of JHs[26]. To determine
179 whether Jhamt functions downstream of Hmgcr in PGC migration, we tested for genetic
180 interaction two ways. First, we measured the effect of genetic *hmgcr* reduction in sensitized
181 *jhamt* heterozygous animals and found that significantly more PGCs failed to reach the gonad in
182 *jhamt*$^{+/-}$; *hmgcr*$^{+/-}$ heterozygous embryos than embryos heterozygous for *jhamt* alone (**Fig 2f**).
183 Second, we tested whether genetic reduction of Jhamt can suppress the ability of ectopic
184 Hmgcr expression to misdirect PGCs. Indeed, loss of one wild type *jhamt* copy reduced the
185 number of PGCs misdirected by Hmgcr (**Fig 2g**). Together, these data suggest that *jhamt*
186 functions downstream of *hmgcr* to direct PGC migration to the somatic gonad.
187
188
189 <u>Juvenile hormone is sufficient for germ cell migration</u>
190
191 Hmgcr is sufficient to direct migrating PGC to many tissues, even far from the normal path, such
192 as to the central nervous system (**Fig 3a** and **Supp Fig 3a**) [20, 27]. To determine whether, like
193 Hmgcr, Jhamt is sufficient for germ cell migration *in vivo*, we ectopically expressed *jhamt* using
194 the GAL4/UAS system. Indeed, PGCs localize near neuronal Elav-positive cells when *UAS-*
195 *jhamt* is induced by *Elav-GAL4*, including to the central nervous system (**Fig 3a**). However,
196 significantly fewer PGCs are misdirected by ectopic *jhamt* compared to ectopic *hmgcr* driven by
197 the same *Elav-GAL4* (**Fig 3b**). Moreover, ectopic *jhamt* expression is not sufficient to drive
198 PGCs to inappropriate locations when *UAS-jhamt* is induced by the endodermal driver, *48Y-*
199 *GAL4*, or the pan-mesodermal drivers, *twist-GAL4* and *24B-GAL4*, even though ectopic *hmgcr*
200 expression with these same GAL4 drivers mislocalizes PGCs (**Supp Fig 3a**). Thus, Jhamt is
201 sufficient to guide germ cell migration *in vivo* in at least one, but not all, tissues.
202
203 Hmgcr is the rate-limiting enzyme in the mevalonate pathway upstream of JH biosynthesis[28].
204 Therefore, tissue-specific differences in Hmgcr expression[20] may underlie the observed context-

205 dependent differences in the ability of ectopic *jhamt* to misdirect PGCs. To circumvent this
206 biological limitation to assess necessity and sufficiency, we turned to an *in vitro* transwell
207 migration assay. In this assay, *Drosophila* PGCs are enriched by fluorescence-activated cell
208 sorting (FACS), placed on a porous filter across media. Previous work had shown that PGCs
209 will translocate across the filter in response toward serum-free culture media conditioned with
210 Kc167 cells[29] (**Fig 3c**). To determine the requirements of JH in this *in vitro* migration assay, we
211 reduced *jhamt* mRNA levels in Kc167 cells using two, independent dsRNAs (Supp Table 3).
212 Like Hmgcr depletion[29], significantly fewer PGCs translocated in response to media that was
213 conditioned by Kc167 cells depleted Jhamt compared to control conditioned medium (**Fig 3d**).
214 Reduced translocation of PGCs could be due to either reduced production in pro-migratory
215 factors or reduced Kc167 cell numbers upon Jhamt knockdown. As such, we measured Kc167
216 number at the end of *jhamt* knockdown and before collection of conditioned media, finding
217 Jhamt depletion had no effect on Kc167 cell number (**Supp Fig 3b**). These data indicate that
218 Jhamt is required for somatic cells to induce PGC migration *in vitro*.
219
220 With a suitable *in vitro* migration system in place, we next sought to directly determine whether
221 JH alone is sufficient for PGC migration. To this end, FACS-enriched PGCs were placed on the
222 transwell membrane above serum-free, unconditioned culture media supplemented with
223 commercially available JH III with 1% BSA as a non-specific carrier protein. We found that
224 PGCs translocated in response to JH III in a dose-dependent manner, such that increased JH III
225 increased PGC translocation except at the highest dose tested (**Fig 3e**). To test the specificity of
226 this response, we subjected PGCs to the JH III analogue and insecticide, methoprene, and
227 found that germ cells translocated in response to methoprene at levels comparable to JH III (**Fig**
228 **3f**). JH signaling is intertwined with the small steroid hormone, ecdysone, which has known
229 roles in the migration of many cell types, including ovarian somatic cells[30, 31]. Therefore, we
230 tested whether PGCs translocated in response to the bioactive form of ecdysone, 20-
231 hydroxyecdysone and found that PGCs did not translocate at any biologically active dose tested
232 (**Fig 3e, Supp Fig 3c**). Together, these data demonstrate that JHs are sufficient to induce PGC
233 migration.
234
235
236
237
238

239 Juvenile hormones impact germ cell migration beyond the canonical transcriptional pathway
240
241 Classical JH signaling involves direct transcriptional responses via nuclear JH receptors (JHNR)
242 (**Fig 4a**)[23]. To determine whether JHNRs are required for PGC migration, we analyzed embryos
243 mutant for two functionally redundant JHNRs, Met and Gce. Existing *met*^{27}*, gce*$^{2.5k}$ mutant
244 animals die during larval development[32]. Therefore, to obtain embryos which lack maternal
245 contributions of Met and Gce, we generated new *met, gce* double mutants that lack *gce* mRNA
246 (**Supp Fig 4a,b**) and carry a point mutation in *met* that garners animals 33x more resistant to
247 methoprene-mediated lethality[33]. When this strain is crossed to *met*^{27}*, gce*$^{2.5k}$ animals under
248 non-crowding conditions, ~5% of the expected class of heteroallelic *met, gce* double mutant
249 animals eclose. As expected[32], we found that fecundity of these escaper *met, gce* females was
250 significantly reduced (**Supp Fig 4c**) but sufficient to analyze the requirements of Met and Gce in
251 embryonic germ cell development. Quantification revealed an increased number of
252 extragonadal PGCs in maternally and zygotically mutant *met, gce* mutant embryos compared to
253 wildtype embryos (**Fig 4b,c**). Analysis of embryos lacking either maternal or zygotic Gce and
254 Met revealed a partial rescue in the number of extragonadal PGCs, which is consistent with an
255 autonomous requirement in PGCs for gonad colonization. However, unlike in *jhamt* and *hmgcr*
256 mutant embryos where germ cells are found posterior to the gonad, we observed that
257 extragonadal PGCs in *met, gce* double mutant embryos were often central and anterior to the
258 gonads, suggesting that PGC migration may be compromised earlier than in *hmgcr* or *jhamt*
259 mutant embryos (**Fig 4b**).
260
261 To further interrogate autonomous requirements for JHNRs in PGCs, we took advantage of our
262 observation that ectopic endodermal Hmgcr expression traps 50-80% of PGCs in the gut at
263 Stage 10 (**Fig 4d**), when PGCs primarily rely on maternally-deposited mRNAs[3]. We thus tested
264 whether maternal loss of Met and Gce suppressed the ability of ectopic *Hmgcr* expression to
265 trap germ cells by crossing wildtype or *met, gce* double mutant females to males containing
266 *48Y-GAL4* and *UASt-hmgcr* transgenes. Quantification of the percentage of PGCs remaining in
267 the gut after gonad colonization revealed a small, but statistically significant decrease when
268 PGCs were maternally mutant for Met and Gce (**Fig 4d,e**). As many PGCs derived from *met,*
269 *gce* mutant mothers were still trapped in the gut by ectopic *hmgcr* expression, these data
270 suggest that either Met/Gce in PGCs is zygotically transcribed and translated in time to respond
271 to ectopic Hmgcr or that the requirements for these JHNRs in PGC migration is non-
272 autonomous.

273 Classical JH signaling culminates in the induction of transcription. To determine whether
274 transcription is autonomously required in PGCs to respond to JH, we utilized the *in vitro*
275 migration assay, which allows us to restrict transcriptional inhibition to PGCs. As expected[34],
276 flavopiridol rapidly and robustly inhibited transcription in PGCs enriched by FACS (**Supp Fig**
277 **4d**). We then subjected control and transcriptionally-deficient PGCs to conditioned media,
278 serum-free media, or serum-free media containing JH III and found that inhibition of
279 transcription did not alter PGC translocation in response to any condition tested (**Fig 4f**). These
280 data suggest that classical transcription-dependent signaling is not required for the migratory
281 response of PGCs to JH.
282
283 JHs can induce rapid biological responses through signaling at the plasma membrane[35-37]. One
284 class of plasma membrane signaling factors implicated downstream of JH in several
285 pharmacological studies are phospholipase C proteins (PLCs)[38-41]. The *Drosophila* genome
286 encodes one gamma PLC, small wing, and two beta PLCs: Plc21c and no receptor potential A
287 (norpA). All three *Drosophila* PLCs are not required for viability, allowing us to examine PGC
288 migration in embryos lacking maternal and zygotic contributions of each PLC. Thus, we
289 examined embryos carrying heteroallelic combinations of existing mutations in *small wing*,
290 *norpA*, and *plc21c*. Somatic defects in *small wing* embryos precluded our investigation into its
291 effect on PGC colonization, as defects in somatic patterning indirectly compromises PGC
292 colonization[42]. Quantification of extragonadal PGCs revealed a mild migration defect in some
293 *norpA* mutant embryos but a significantly stronger PGC migration phenotype in *plc21c* mutant
294 embryos (**Fig 4g,h**). Similar to *jhamt* and *hmgcr* mutant embryos, extragonadal PGCs in *plc21c*
295 mutant embryos were found within the mesoderm posterior to the gonad, suggesting a failure in
296 the second step of PGC migration (**Fig 4g,h**). To test whether Plc21c functions within PGCs to
297 respond to Hmgcr/JH, we crossed *plc21c* mutant females to males carrying *48Y-GAL4* and
298 *UAS-hmgcr* transgenes and quantified the percentage of PGCs trapped in the endoderm. These
299 experiments revealed that maternal loss of Plc21c suppress the number of PGCs trapped in the
300 endoderm by ectopic Hmgcr expression (**Fig 4i,j**).Together, these results suggest that JH
301 facilitates PGC migration to the gonad through non-transcriptional signaling that includes Plc21c
302
303
304
305
306

307 Role of bioactive isoprenoids in early germ cell development may be broadly conserved

308

309 Insect JHs and vertebrate retinoic acids (RAs) have pleiotropic functions throughout the
310 germline lifecycle. However, a role in germ cell migration had not previously been described for
311 either bioactive isoprenoid. JHs and RAs are capable of cross-activating respective
312 transcriptional signaling cascades[43]. To determine whether *in vitro* cross activation extends to
313 PGC migration, we isolated *Drosophila* germ cells by FACS and subjected them to JH III or to
314 two RA species, all-trans retinoic acid (ATRA) or 9-cis RA. Notably, 9-cis RA induced
315 *Drosophila* germ cell translocation to levels comparable of JH III (**Fig 5a**). These data show that
316 RAs are capable of inducing PGC migration in *Drosophila*, suggesting commonality in PGC
317 response to bioactive isoprenoids.

318

319 Enzymes critical for biosynthesis of RAs are expressed in the developing bipotential somatic
320 genital ridge of mouse embryos[7]. To determine whether RAs may have a similar role in
321 vertebrate germ cell development, we adapted the *in vitro* transwell migration assay developed
322 for *Drosophila* PGCs to mouse germ cells. To this end, we obtained mouse germ cells by FACS
323 from embryonic day 10.5 embryos carrying a germ cell-specific transgene (*Oct4ΔPE::GFP*). We
324 exposed germ cells to fetal bovine serum in PGC media as a positive control or serum-free PGC
325 media as a negative control. Strikingly, both ATRA and 9-cis RA induced translocation of mouse
326 embryonic germ cells to levels comparable to the known mouse PGC chemoattractant, C-X-C
327 Motif Chemokine Ligand (CXCL12) (also called SDF1a) (**Fig 5b**)[44-46]. Importantly, while RAs can
328 have a proliferative effect on mouse PGCs, this effect was reported over 24-72 hours[47].
329 Consistently, we did not detect PGC proliferation in response to RAs during our two-hour *in vitro*
330 migration assay, indicating the increased number of translocated PGCs was not due to RA-
331 induced proliferation (**Supp Fig 5b**). Together, these data suggest that the newly uncovered
332 role of secreted isoprenoids in early germ cell guidance may be broadly conserved among
333 invertebrate and vertebrate species.

334

335

336

337

338

339

340

341 **Discussion**

342

343 The bioactive isoprenoids RAs and JHs impact the germline lifecycle in multiple and complex
344 ways across the animal kingdom. Here we provide the first evidence that bioactive isoprenoids
345 act earlier during germ cell development than previously described. Our results suggest that
346 bioactive isoprenoids guide migrating PGCs to colonize the somatic gonad (**Fig 5c**). In contrast
347 to established endocrine, transcription-dependent mechanisms, we show that JHs facilitate
348 PGC migration locally within the mesoderm through transcription independent mechanism. Our
349 studies using *Drosophila* significantly expand the scope and mechanisms by which JHs impact
350 reproductive development. Our studies of RAs and mouse germ cells suggest that these new
351 functions for bioactive isoprenoids may be broadly conserved.

352

353

354 <u>JH functions locally in *Drosophila* embryogenesis</u>

355

356 Investigations into JH biology have largely focused on systemic, endocrine-mediated effects on
357 juvenile development and adult fertility. Our study uncovered an embryonic function for JH that
358 precedes development of the endocrine gland thought to be the principal source of JH in
359 insects[19, 22]. Interestingly, instead of systemic JH activity throughout the embryo, we find that JH
360 signaling in *Drosophila* mid-embryogenesis occurs within a thin mesodermal strip along the
361 germband (**Fig 1e, Supp Fig 1c**). Although local JH signaling could reflect tissue-specific
362 differences in transduction capability, both JHNRs and their co-factor Taiman are maternally
363 provided[48, 49]. Thus, we favor a model in which expression of the key JH biosynthetic gene,
364 *jhamt* and JH reporter activity within the mesoderm reflects local production and paracrine
365 signaling (**Fig 1b,e**). Evidence for local JH activity in adult *Drosophila* intestines[50] and germline
366 stem cell niches of adult *Drosophila*[51] has been described, with the caveat that many gonadal
367 Gal4 drivers are also active in the nervous system[52]. Our data build on these recent findings and
368 suggest that JH functions in a short range, paracrine manner, similar to the mammalian
369 bioactive isoprene RA. To generate instructive spatiotemporal differences, RA gradients form
370 through dynamic changes in expression of RA biosynthesis and degradation enzymes.
371 Curiously, degradation enzymes for both RA and JH exhibit strikingly similar dynamic and sex-
372 specific expression patterns[17]. Together, these finding suggest that spatial JH dynamics may be
373 instructive to PGCs. Consistent with this postulate, we found that in addition to PGC migration
374 defects, *met, gce* double mutant larvae have markedly increased titers of JH III and JHB_3 (**Supp**

375 **Fig4e**). It will be important to determine whether, like RA, spatial JH dynamics are instructive to
376 PGCs during embryogenesis.
377
378
379 PGCs respond to JH through non-canonical signaling
380
381 Classic JH and RA signaling involves nuclear receptor-mediated transcription. Curiously, we
382 find that PGCs respond to JHs even when transcription is globally inhibited (**Fig 4f**), suggesting
383 that PGCs respond to JH through rapid, non-transcriptional mechanisms. Rapid, non-
384 transcriptional responses to JH during ovarian follicle development have been postulated for
385 decades[36, 53-55], however the precise mechanisms have been more elusive. Consistent with
386 pharmacological-based studies that implicate plasma membrane receptors, Protein Kinase C
387 and PLC[38-41], our data suggest that Plc21c is involved in JH-mediated PGC colonization of the
388 gonad (**Fig 4g,h**). As a beta type PLC, Plc21c is linked to G protein-coupled receptors
389 (GPCRs). GPCRs have a prominent role in cell migration and GPCR-mediated desensitization
390 could account for our observation that *in vitro* migration is reduced in response to higher JH
391 concentrations (**Fig 3e**). A GPCR that binds JH has not been identified in *Drosophila*, though
392 putative JH GPCRs have been identified in other insects[56]. Identification of the GPCR that
393 mediates JH, or RA signaling, in early PGC development and other reproductive processes will
394 be an exciting area of future exploration.
395
396
397 Bioactive isoprenoids in cell migration
398
399 The timing, modality, and directionality of cell migration is dictated by extracellular information.
400 The regulation of such parameters is particularly important when cells are migrating within the
401 context of a developing tissue or animal. Our investigations revealed that extracellular JH
402 ensure migrating PGCs reach the embryonic somatic gonad. To our knowledge, such a role for
403 JHs has not been previously described. Intriguingly, ecdysone, the insect hormone that is
404 functionally opposed by JH signaling in larval development, governs the timing, motility, and
405 organization of several ovarian somatic cells in *Drosophila*[30, 31, 57]. Ecdysone signaling is not
406 active in the *Drosophila* embryo until Stage 13, where it is first active in the amnioserosa far
407 from developing gonads[58]. Consistently, we did not find evidence that ecdysone impacts PGC
408 migration *in vitro* (**Fig 3e**). However, given the antagonism between ecdysone and JHs in other

biological contexts and the coordinated nature of germ cell and somatic gonad development[57, 59-61], it will be important to determine whether JH dynamics impact the migration of somatic gonadal cells.

Results presented here suggest that JHs directly impact PGC migration. While JHs have not been implicated cell migration, the same is not true for retinoids. While most investigations into the role of RAs in cellular migration have focused on transcription-based mechanisms that upregulate receptors required for homing [62, 63], evidence for transcription-independent functions of RAs is also emerging[64]. RAs facilitate axon guidance in *Xenopus laevis*[65], and in snails through non-transcriptional mechanisms involving calcium flux, Rho GTPases and G proteins[66-69]. Our studies also implicate G protein, calcium signaling and leave open the possibility that cytoplasmic signaling axis is broadly shared across bioactive isoprenoids. Consistently, we find that RAs are sufficient to induce mouse germ cell migration *in vitro* (**Fig 5b**). Unlike previous *in vitro* migration assays done on mouse embryonic germ cells[46, 70, 71], our transwell incubation period for mouse PGCs was only two hours. This short temporal window is suggestive of a rapid response by mouse PGCs downstream of RAs, but future work will be needed to determine whether the impact of RA on mouse germ cells requires transcription, RA nuclear receptors or PLC-based signaling.

<u>A cohesive class of bioactive isoprenoids in reproductive development</u>

In total, our findings support a hypothesis that JHs and RAs are functionally analogous molecules in reproductive development. Beyond similar roles in post-meiotic gametogenesis[72, 73], we provide evidence that, like RAs, JHs act in a paracrine manner to support embryonic reproductive development. Like JH, RA biosynthesis enzymes are expressed during PGC gonad colonization,[7] and after PGC colonization, degradation enzymes are induced specifically in male gonads in *Drosophila* and mice. RA was recently implicated in sex-specific differentiation of the gonad[9], which may be akin to the role of the bioactive isoprenoid, methyl farnesoate, in crustacean sex determination [6, 74]. Given these similarities, we assert that *Drosophila* can serve as a powerful model to understand how bioactive isoprenoids impact embryonic reproductive development. Such additional genetic models are needed, as recent investigations have brought the role of RA in early reproductive development into question[7, 8, 13 11, 14, 15, 75]. *Drosophila* is a simplified and tractable model in which to tease apart primary

443 functions and molecular mechanisms to understand the full breadth of isoprenoid impact on
444 reproductive development.
445
446
447 **Acknowledgements**
448
449 We thank Marek Jindra and Ryusuke Niwa for reagents and discussions, and Peter Nicholls and
450 David Page for instructive discussions on mammalian reproductive development and assay
451 development. We are grateful to Alexey A Soshnev for graphical designs, Cesar Ramirez and
452 Francisco Fernandez-Lima for assistance with mass spectrometry. We are especially grateful to
453 Rebecca Spokony, Jessica Treisman, Pamela K Geyer, and Toby Lieber for valuable advice
454 and insightful discussions, as well as all members of the Lehmann laboratory for valuable input.
455 Stocks obtained from the Bloomington Drosophila Stock Center (NIH P400D018537) were used
456 in this study. In addition, several monoclonal antibodies used in this study were obtained from
457 the Developmental Studies Hybridoma Bank, created by the NICHD of the NIH and maintained
458 at The University of Iowa, Department of Biology, Iowa City, IA. We also thank the NYULMC
459 Core Cytometry Facility, which is partially funded by NIH/NCI P30CA016087. This work was
460 supported by a Damon Runyon Cancer Research Foundation postdoctoral fellowship from the
461 William Raveis Charitable Fund (DRG2235-15, L.J.B), an NIH Pathway to Independence award
462 (K99 HD097306, L.J.B.), an NIH-NIAID R01 award (R01AI04554, F.G.N), and NIH-NIAID R21
463 award (R21AI153689 to M.N.) and an NIH MERIT award (R37HD41900, R.L). RL was a HHMI
464 investigator.
465
466
467 **Author Contributions**
468
469 Conceptualization: LJB, RL; Experimentation: LJB, JS, EPD MN, FGN, MS; Analysis: LJB, MN,
470 FGN; Writing: LJB, RL; Funding Acquisition: LJB, RL; Supervision: LJB, MS, RL
471
472
473 **Declaration of Interest**
474
475 The authors declare no competing interest
476

Materials and Methods

Animal Maintenance

Drosophila melanogaster were raised on medium containing 1.5% yeast, 3.6% molasses, 3.6% cornmeal, 1.12g Tegosept, 1.12% alcohol and 0.38% propionic acid. For embryo collections, apple juice plates contained 25% apple juice, 2.5% sucrose, 2.25% bactoagar, 0.15% Tegosept. Animals were kept at 25°C for all experiments. Fly strains used in this study are listed in Supplementary Table 1.

Mice expressing a germ cell-specific *Oct4ΔPE::GFP* transgene[76] (B6; CBA-Tg(Pou5f1-EGFP)2Mnn/J) were obtained from Jackson Laboratory (#004654, Bar Harbor, ME, USA). All protocols were approved by the NYU Institutional Animal Care and Use Committee.

Generation and validation of the P[*JHRE-GFP, w+]* transgenic reporter

Eight copies of the wildtype JH response element (JHRE) from the *early trypsin* gene from *Aedes aegypti*[24], or eight tandem copies of the mutant JHRE (Supp Fig 1), were excised from *pGL4.17* vectors provided by Jindra Marek. JHREs were inserted upstream of the minimal *hsp70b* promoter and *eGFP* coding sequence of pS3aG transformation vector (Addgene #31171) containing an *attb* for site-specific integration. JHRE reporter constructs were integrated into *y+, attP2* at cytological position 68A4 sites by Bestgene.

To validate the JHRE-GFP reporter, transgenes were placed in met^{1}, gce^{MI} mutant background. Embryonic GFP signal was measured by immunohistochemistry (Supp Fig 1). To measure JH responsiveness, first instar larvae were placed in food containing 1.6ug of methoprene per gram of food [77], or ethanol as a control for 24 hours. *GFP* mRNA was measured in whole second instar larvae by qPCR using primers in Table 3 (Fig 1 and Supp Fig 1).

Generation of *jhamt* alleles

The crispr guide CCTGGATGTGGTTCAGGATCT was cloned into pU6-2 gRNA vector (DGRC #1363) and injected into embryos into a stock derived from BL51324 carrying w^{1118} ;; *PBacy[mDint2]=vas-cas9VK00027* by Bestgene. Of 29 fertile founders, 87 F1 crosses were set up and screened for *jhamt* mutations by PCR amplification and Sanger sequencing using primers listed in Table 3. Of 48 F1 lines screened, 13 lines were obtained wherein small indels created a frame shift just before the methyltransferase domain, which starts at amino acid 40, leading to a stop codon just downstream, two lines at amino acid 46 (12F1 and 12F2) and the remaining lines at amino acid 54 (1F1, 1F2, 4F1, 4F3, 6F3, 7F2, 7F3, 8F1, 8F2, 12F3, 14M2, 14M3). Nonsense mediated decay was detected in all lines by measuring *jhamt* mRNA in whole adult animals by qPCR (Supp Fig 2a). The new alleles on JH III and JHB_3 titers were quantified in third instar larval hemolymph (See separate subsection in Methods).

522 Embryo Immunofluorescence
523 Prior to embryo collection, young parental strains (less than 5 days old) were mated in vials for
524 one day before transferring to embryo collection cages containing apple juice plates and wet
525 yeast. Embryos were dechorionated in 50% bleach for three minutes, rinsed with water and
526 fixed in a scintillation vial containing 2ml of 4% formaldehyde in PBS and 8ml of heptane.
527 Embryos were fixed for 20 minutes on a shaker. To remove the vitelline membrane,
528 formaldehyde was removed from the scintillation vial and 10ml methanol was added, followed
529 by one minute of vigorous shaking by hand. Embryos were washed with fresh methanol three
530 times before storage at -20C or future processing.
531
532 For immunohistochemistry, embryos were sequentially rehydrated with increasing percentage of
533 PBSTx (PBS with 0.1% TritonX100) and then washed six times with PBSTx before a one-hour
534 block using 1% BSA in PBSTx at room temperature. Primary antibodies were incubated
535 overnight at 4C and then washed six times in PBSTx. Secondary antibodies in 1% BSA in
536 PBSTx were incubated for two hours at room temperature, washed six times in PBSTx.
537 Embryos were then equilibrated in Vectashield (Vector Laboratories, H-1200) overnight at 4ºC
538 before mounting on coverslips.
539
540 Fluorescent *in situ* hybridization was done as previously shown[78]. Probes were generated using
541 *Drosophila* clones from DGRC (*jhamt* #11840, clone AT13581) and (*Nano*s #1124533, clone
542 RE53469).
543
544
545 mRNA quantification by qPCR
546 RNA was obtained by TRIzol (Invitrogen #15596018) extraction. DNA was removed using RQ1
547 RNase-Free Dnase (Promega #M6101). cDNA was generated using SuperScript III Reverse
548 Transcriptase (Fisher Scientific #18080-044) using both oligo dT and random hexamers.
549 Primers used are listed in Table 3. qPCR was carried out using LightCycler 480 SYBR Green I
550 Master 2X (Roche #04887352001) and a Roche LightCycler 480 machine. Results were
551 calculated as previously described[79] from crossing points and normalized to one of three
552 reference genes found to have invariant expression across tissues and developmental stages:
553 *DCTN2-p50*, *und*, *DCTN5-p25*[80].
554
555
556 Evaluation of JH titers by quantitative mass spectrometry
557 The following genetic backgrounds were used to measure JH III and JHB_3 titers:
558 *jhamt*$^{8F2/12F1}$ paired with the *w*^{118}*; CyO, ft-lacZ* genotype, which was the genetic background the
559 crispr alleles were extensively crossed into and *gce*^{Mi}*, met*^{1} paired with *w*^{118}. Twenty-five third
560 instar larvae per biological replicate were collected from sparsely populated vials, washed in
561 PBS before placing in 50µl of pre-chilled PBS for hemolymph collection. To collect hemolymph,
562 the cuticle was pinched and pulled apart down the length of the animal. Care was taken not to
563 rupture fat body or intestines. Hemolymph was transferred to pre-chilled silanized glass vials
564 (Fisher Scientific #C4011S5 and #C401154B) using silanized glass pipettes (Brain Bits #FPP).
565 The glass collection well was rinsed with 50µl additional, pre-chilled PBS to obtain any

566 remaining hemolymph and additional PBS was added to silanized glass vial for a total volume of
567 150µl. Deuterated JH III (62.5pg) dissolved in acetonitrile (Thermo Fisher #51101) was added to
568 each replicate, then 600µl hexane (Sigma Aldrich #1037011000). Samples were vortexed for 1
569 minute and centrifuged for 5 min at 2000g at 4C. Organic phase was transferred to new
570 silanized vial for analysis by mass spectrometry.
571
572 For mass spectrometry analysis, the JH III and JH III bisepoxide (JHB_3) amounts present in
573 hemolymph were quantified by liquid chromatography coupled to tandem mass spectrometry
574 (HPLC-MS/MS)[25]. The identification and quantification of JH III and JHB_3 in hemolymph
575 samples was based on multiple reaction monitoring (MRM), using the two most abundant
576 fragmentation transitions: for JH III: 267->235 (primary) and 267->147 (secondary), and for
577 JHB_3: 283->233 (primary) and 283->251 (secondary)[25].
578
579
580
581 Fecundity measurements
582 Fecundity was measured as previously described[81] and reported as the average number of
583 eggs laid in three- and four-day old females at 25ºC. In each biological replicate, 10-12 females
584 were crossed to 5-6 w^{118} males to mitigate male fertility defects upon *jhamt* loss.
585
586
587
588 Knockdown of *jhamt* in Kc167 Cells
589 To target *jhamt*, genomic DNA obtained from Kc167 cells using Qiagen's Blood and Tissue Kit
590 (#69506) was used as a template. To target lacZ, pBluescript SK plasmid used as a template.
591 dsDNA was generated by Choice Taq Mastermix (Denville Scientific #CB4070-8). Gradient PCR
592 was used to obtain optimal dsDNA templates. dsRNAs were generated from dsDNA templates
593 using T7 MEGAScript (Invitrogen #am1334) according to standard protocol. dsRNAs were
594 DNAse treated (Qiagen #79254) and purified using Qiagen RNAeasy Mini Kit (Qiagen #74104)
595 according to instructions. For transfection, Kc167 cells were grown to confluency, resuspended
596 in fresh Schneider's media (Fisher #21720-001) supplemented with Penn/Strep (Fisher,
597 #15140122) and 10% heat inactivated FBS (Thermo Fisher #16140071) to 1x10^6 cells/ml and
598 allowed to settle overnight. 2µg of dsRNAs were used in conjunction with Effectene Transfection
599 Reagent (Qiagen #301425) into each 6-well dish. After 48 hours at 25ºC, media was removed,
600 transfected Kc167 cells were washed in PBS and resuspended in serum-free Schneider's Media
601 (with Penn/Strep) for three additional days at 25ºC prior to collection of Kc167-conditioned
602 media. To determine whether *jhamt* knockdown compromised Kc167 viability, the number of
603 Kc167 cells was counted on the day conditioned media was collected. Knockdown efficiency
604 was determined in Kc167 cells by qPCR when conditioned media was collected for the transwell
605 assay. Primers were chosen outside of region targeted by dsRNAs.
606
607
608
609

610 Isolation of PGCs
611 *Drosophila* embryos carrying the *P[nos-Moe::eGFP.nos 3'UTR]* transgene from an overnight
612 collection were dechorionated in 50% bleach for two minutes, rinsed and placed in filter-
613 sterilized Chan and Gehring's Balanced Saline, PGC Sort Buffer (3.2g/L NaCl, 3.0g/L KCl,
614 0.69g/L CaCl2.2H2O, 3.7g/L MgSO4.7H2O, 1.79g/L Tricine buffer (pH 7), 3.6g/L glucose,
615 17.1g/L sucrose, 1g/L BSA, fraction V). Dechorionated embryos were manually homogenized in
616 PGC Sort Buffer with Dounce homogenizer (Pyrex #7727-15) and passed through a 100µm filter
617 and 20µm filter and placed in pre-chilled polypropylene falcon tubes (#352063). Live, GFP-
618 positive *Drosophila* PGCs were sorted using a MoFlo XDP cell sorter fitted with a 70µm nozzle
619 into Maxymum recovery microtubes (Axygen #311-05-051) containing 200µl Schneider's Media.
620
621 To enrich for mouse PGCs, B6; CBA-Tg(Pou5f1-EGFP)2Mnn/J (Jax #004654) mice were bred
622 to produce embryos homozygous for the *Oct*Δ4PE::GFP transgene. Embryonic day 0.5 (E0.5)
623 was assumed to be noon of the day the vaginal plug was observed. Pregnant females were
624 euthanized by carbon dioxide followed by cervical dislocation. Trunks were dissected from
625 E10.5 embryos in chilled PBS. For each two embryos, tissue was dissociated in 300µl of 0.5%
626 trypsin (0.25%, Life Technologies #25200056) for 15 min at 37ºC, with occasional manual
627 disruption by pipette. Trypsin was inactivated with 200µl of mouse PGC culture media
628 [DMEM/F-12 (Thermo Fisher #11-320-033), 250µM sodium pyruvate (Thermo Fisher
629 #11360070), 2mM L-glutamate (Gibco #25030081), 1X MEM Non-essential amino acids
630 (Thermo Fisher #11-140-050) containing 25% Bovine Albumin Fraction V (Thermo Fisher
631 #15260037). Dissociated tissue was centrifuged at 200g for 7 min and cells were resuspended
632 in 2mL of PGC media. Cell suspension was filtered through a 35µm cell strainer into a 5 ml
633 falcon round bottom tube (VWR #21008-948) for sorting using a MoFlo XDP cell sorter fitted
634 with a 100µm nozzle. Live, GFP+ germ cells were sorted into Maxymum recovery microtubes
635 (Axygen #311-05-051) containing mouse PGC media.
636
637
638 *in vitro* Migration Assays
639 For *in vitro* transwell assays, all plastic ware, tips, tubes and transwell plates used throughout
640 the assay were pre-coated with PBS containing 1% BSA to prevent hydrophobic molecules from
641 sticking to the surfaces. Assays with light sensitive isoprenoids were done in dark conditions as
642 much as possible. For Kc167-conditioned media, serum-free media was added to washed,
643 confluent Kc167 cells and collected three days later. Conditioned media was collected and
644 centrifuged 4,000rpm for 20 min to remove all cellular debris and placed on ice. All isoprenoids
645 (Supplementary Table 4) were prepared by dilution series in either serum-free Schneider's
646 media for *Drosophila* PGC assays or mouse PGC media. Transwell assays were done using the
647 96-well ChemoTx Disposable Chemotaxis System (NeuroProbe #116-10) which had a standard
648 PCTE filter membrane with 10µm pore size, 300µl well capacity and 5.7mm cell site diameter.
649 Sorted germ cells recovered on ice for 30 min while the transwell system was set up. Sorted
650 germ cells were then diluted 10-15-fold in serum-free Schneider's media for *Drosophila* PGC
651 assays or mouse PGC media so that 60µl diluted PGCs were placed above each well.
652 Transwell plates with *Drosophila* PGCs were incubated 25ºC for 1.5 hours and those with
653 mouse PGCs were incubated at 37ºC for 2 hours. After the incubation period, PGCs were

654 removed from above membrane, the plate was centrifuged at 460rpm for 10min to dislodge cells
655 from the well side of the membrane. Translocated germ cells were removed from the 96-well
656 plate by pipetting up and down and transferring to Nunc Lab-Tek II Chambered Coverglass
657 (Thermo Fisher #155409) for manual quantification by fluorescent microscopy.
658
659 The number of PGCs in each top well was calculated by setting aside 10% input (6µl) in
660 duplicate into Lab-Tek wells, each with 300µl serum-free media at the beginning of the transwell
661 assay and quantifying the number of germ cells when the experimental translocated germ cells
662 were quantified. To compare biological replicates done on different days, Specific Migration was
663 calculated by first subtracting the number of germ cells that translocated in the negative control
664 wells (serum-free media) and then calculating the percentage of normalized experimental
665 condition to the respective positive control. Each transwell assay is the result of two to four
666 biological replicates, each consisting of two technical replicates.
667
668
669 Verification of Hormone Activity *in vitro*
670 To verify the activity of JH III and 20-hydroxecdysone (Supplemental Table 4), hormones were
671 added to 50% confluent Schneider 2 (S2) cells at the concentrations indicated in Supp Fig 3d.
672 After a six-hour incubation at 25ºC, S2 cells were harvested and mRNA was extracted and
673 analyzed using protocols described in the '*mRNA quantification by qPCR*' Methods subsection.
674
675
676 Transcription Inhibition in *Drosophila* PGCs
677 Efficient inhibition of transcription in Drosophila PGCs isolated by FACS was determined by
678 testing different concentrations of Actinomycin D and Flavopiridol (See Supplemental Table 4).
679 To visualize transcription by immunohistochemistry, Lab-Tek II 8-chambered coverglass were
680 incubated with poly-L-Lysine solution (Sigma-Aldrich #P4707) for 30 min at room temperature
681 and then dried for 1.5 hours. Sorted *Drosophila* PGCs were added to chambers and incubated
682 with Actinomycin D or Flavopiridol for either 15 min or 3 hours, then fixed with 4%
683 paraformaldehyde for 15 minutes, washed in 0.05% PBS with TritonX100, blocked in 1% BSA
684 for 30 min and stained for Vasa, RNA Pol II Ser2CTD and RNA Pol II Ser5 CTD (See
685 Supplemental Table 2 for antibody information). As expected[34], Flavopiridol rapidly inhibited
686 transcription in *Drosophila* PGC while not compromising cell viability. For transwell assays,
687 sorted *Drosophila* PGCs were first incubated with 1µM Flavopiridol for 30 min prior to placing on
688 transwell membrane and solutions in the bottom well chambers also contained 1µM Flavopiridol
689 to ensure PGC transcription was inhibited throughout the assay.
690
691
692 Microscopy and Image Processing
693 Most embryos and other samples were imaged with a Zeiss LSM800, an upright laser scanning
694 confocal microscope using Zen Blue 2.3 software and a Plan-Apochromat 20x0.8 NA air
695 objective and 40x1.3NA oil objectives with pinhole size for all imagine was set to 1AU. Images
696 were processed using ImageJ.
697

698 Statistics
699 Statistical analysis was done as described in the Figure Legends. Briefly, for quantification of
700 phenotypic data, such as extragonadal PGC quantification, data was not always normally
701 distributed and thus median +/- IQR are reported and statistical significance was assessed by
702 Mann-Whitney U test. For mRNA Fold Change and *in vitro* Specific Migration results, mean +/-
703 standard deviation is reported and statistical significance was tested by unpaired t-test. Sample
704 size per biological replicate was influenced by power analysis based on previously observed
705 phenotypic variation.
706
707
708
709
710
711
712
713
714
715
716
717
718
719
720
721
722
723
724
725
726
727
728
729
730
731
732
733
734
735
736
737
738
739
740
741

742 **Supplemental Table 1:** Animal lines used in this study
743

Name	Species	Source	Notes
P[JHREWt8x-eGFP]attp2	*Drosophila*	This study	JH responsive reporter, with non-specific activity in hemocytes
P[JHREMut8x-eGFP]attp2	*Drosophila*	This study	Negative control reporter transgene with non-specific activity in hemocytes
y^1,w^*, $gce^{mi02742}$	*Drosophila*	BL60189	Insertion that leads to RNA null
met^1	*Drosophila*	BL3472	EMS-generated from OregonR-C causing G1161736A, DNA mutation and G166D protein change, genetically amorphic allele [82 33]
y^+, w^+, v^+, met^1, $gce^{mi02742}$/Fm7ai	*Drosophila*	This study	Recombinant between existing mutants listed above
w-, v-, met^{27}, $gce^{2.5k}$/Fm7ai	*Drosophila*	Rebecca Spokony and Lynn Riddiford [83]	Both met^{27} and $gce^{2.5k}$ are large deletions that lead to full loss of RNA
w^{1118}; $jhamt^{8F2}$ or ^{12F1}/CyO, ft-lacZ	*Drosophila*	This study	crispr generated small deletions
$jhamt^{Df(2L)BSC781}$/CyO, ft-lacZ	*Drosophila*	BL27353	2L:16325113;16417726, including *jhamt* and 13 other genes
$hmgcr^{26.31}$/Tm3, Ubx-lacZ	*Drosophila*	[42]	Also known as clb^2
$hmgcr^{11.54}$/Tm3, Sb, Ubx-lacZ	*Drosophila*	[42]	Also known as clb^1
$hmgcr^{01152}$/Tm3, Ubx-lacZ	*Drosophila*	[20]	L(3)01152 source: Transposon insertion 179 nucleotides into *hmgcr* locus
y^1, w*; $pPlc21c^{Mi}$/Cyo,ft-lacZ	*Drosophila*	BL60761	MI02818 gene trap insertion with a stop codon after amino acid 126[84]
$plc21c^{Df(2L)BSC106}$	*Drosophila*	BL8672	
w^{1118};; $itpr^{P05616}$	*Drosophila*	BL11664	p-element insertion in first exon
w*, $norpA^{36}$	*Drosophila*	BL9048	Ems-induced amorphic, loss of function allele
^{w1118}, $norpA^{Df(1)BSC}$	*Drosophila*	BL26575	X:431805;X4533198,2 includes *norpA* and 14 other genes
w, sl^{K08}	*Drosophila*	[85]	1 bp deletion in exon 1, leading to a premature stop codon at aa28
Ln(1)bbDf, y1, sl^2/Fm4	*Drosophila*	BL724	x-ray induced loss of function allele
UAS-hmgcr	*Drosophila*	[20]	pNB36C *hmgcr* cDNA downstream of UASt
y,w; ; UAS-jhamt	*Drosophila*	Ryusuke Niwa [19]	RN286 and RN287, both on the third chromosome, containing two point mutations also found in w118 (F166Y and S182N)
w^-; elav-GAL4	*Drosophila*	J Treisman	Second chromosome
w^-; 48Y-GAL4	*Drosophila*		Second chromosome
w^-; twi-GAL4; 24B-GAL4	*Drosophila*	M. Akam	Second and third chromosome
y,w;; Tub-GAL4	*Drosophila*		Third chromosome
w-, P[nos-moesin::egfp::nos 3'UTR]	*Drosophila*	[86]	
Oct4ΔPE::GFP	Mouse	Jax #004654	B6; CBA-Tg(Pou5f1-EGFP)2Mnn/J

744
745
746
747
748
749
750
751
752
753
754
755
756

757 **Supplemental Table 2:** Antibodies used in this study
758

Name	Source	Species	Concentration
Vasa	Lehmann lab	Rabbit	1:5,000
GFP	AVES #1020	Chicken	1:500
GFP	Thermo Fisher Scientific #A11122	Rabbit	1:1,000
Singed (fascin)	DSHB #sn 7c	Mouse	1:100
Elav	DSHB #9F8A9	Mouse	1:500
b-galactosidase	Abcam #ab9361	Chicken	1:500
Hindsight	DSHB #1G9	Mouse	1:20
RNA Pol II Ser5	Chromotek #3e8-1	Rat	1:100
RNA Pol II Ser2	Abcam #ab5095	Rabbit	1:500

759
760
761
762
763
764
765
766
767
768
769
770
771
772
773
774
775
776
777
778
779
780
781
782
783
784
785
786
787
788
789
790
791
792

793 **Supplemental Table 3:** Primers used in this study
794

Element	Purpose	Forward Primer	Reverse Primer
jhamt	Genotyping crispr deletions	AGGTGCAAAGGCACGAT	AGGTGCAAAGGCACGAT
jhamt	Crispr guide	CTTCGAGATCCTGAACCCACATCC	AAACGGATGTGGGTTCAGGATCTC
jhamt	*in situ* probe	GGCACGATGCCAAATTGAT	GATAATACGACTCACTATAGGGGATGTGTAGGCTC CAGGAAA
Nanos	*in situ* probe	AGATTGCGCGATCCTTGAA	TAATACGACTCACTATAGGGCTGGATTCGCCCTCT CTAAAC
und	reference gene for qPCR	GCAAGAAAAGCGGTCAGACT	CGTGTTGATACGGTCCAGAG
Dnm/DC TN2-p50	Reference gene for qPCR	AGACGCCTGGAAGTAAGCAG	GTAAGGCGGCTCAACTTGTC
DCTN5-p25	reference gene for qPCR	ACAAAGTTAGTCGCCACACG	ATGACGGAGTTCTTGCCAAT
twinstar	Detect DNA contamination for qPCR	TCAGAGGTGCCTTGACACTG	GATGTGGAGACTGTGGCAGA
eGFP	mRNA quantification	GAACCGCATCGAGCTGAA	TGCTTGTCGGCCATGATATAG
gce	Genotyping *gce* alleles	GGATGCCATCGATCGCAAGT	GCTTCGTCACTACGCCGAAA
met	Genotyping *met*[1] allele	CTGCTTCCTCACCCTAACCT	CTGCTTCCTCACCCTAACCT
jhamt	mRNA quantification	TGACCATGTCACCTCGTTCTACTGC	G AAG T C AT C C AG G A A C T G T T C AT G C
jhamt	dsRNA 1 for knockdown in Kc167 cells	TAATACGACTCACTATAGGGCCTCACGCCT TCATAAACAA	TAATACGACTCACTATAGGGGGTAACGTGCTCATG GACT
jhamt	dsRNA 2 for knockdown in Kc167 cells	TAATACGACTCACTATAGGGCTTCGTAAAG CCACTGCTCC	TAATACGACTCACTATAGGGCCTCGCCAGGACTTA GACTG
lacZ	dsRNA knockdown DRSC42733	TAATACGACTCACTATAGGG CTGGCGTAATAGCGAAGAGG	TAATACGACTCACTATAGGG CATTAAAGCGAGTGGCAACA
jhamt	Knockdown efficiency	CAGTTCCTGGATGACTTCATAGAC	CCA CCA CCA ATT TAT AGG GAG ATA G
kr-h1	JH responsiveness	G AAT AC G AC AT A AC AG C C	CGATTTCCGTGAATATGTTCT
Eip74b	20E responsiveness	GTACGCGTATTGGGACTATCAG	CACGCGAGATAGGGATTTCTT
Eip75	20E responsiveness	GTCCATCAGCGAGTTGGTATC	CACCAGCAGCCATCTGAA
plc21c	Genotype *plc21c*^{K03}	TCGGATACCAACCAGGACTATG	TATCTCGGGCACGAACGTATAG
sl	Genotype *sl*^{K08}	CGGATGAGAACTGGATTCGATAG	GTGCAGTATGACAAAGCACTTG

795
796
797
798
799
800
801
802

803 **Table 4:** Pharmocologics used in this study
804

Name	Source	Product Number	Stock solvent	Final Concentration
JH III	Sigma-Aldrich	J2000-10MG	Ethanol	0.25-25μM
Methoprene	Sigma-Aldrich	33375-100MG	Ethanol	2.5μM
20-hydroxecdysone	Sigma-Aldrich	H5142-5MG	Ethanol	0.25-25μM
ATRA	Sigma-Aldrich	R2625-50MG	DMSO	2.5μM
9cis-RA	Sigma-Aldrich	R4643	DMSO	2.5μM
Flavopiridol	Selleck	S1230	PBS with 0.1% BSA	1μM
Actinomycin D	Sigma-Aldrich	A1410-Smg	DMSO	1-5μg/mL
CXCL12/Sdf-1a	R&D Systems	460-SD-010	PBS with 0.1% BSA	50ng/mL

805
806
807
808
809
810
811
812
813
814
815
816
817
818
819
820
821
822
823
824
825
826
827
828
829
830
831
832
833

834 **Figure Legends**

835

836 **Figure 1: Juvenile Hormone (JH) signaling is present during embryonic germ cell**
837 **development a** Schematic of germ cell development during Stage 10-14 of *Drosophila*
838 embryogenesis. SD stands for sex differentiation. **b** Lateral view images of a late Stage 12
839 embryo stained by Fluorescent *in situ* hybridization (FISH) for *jhamt* (green) and *nanos*
840 (magenta) mRNA. Primers used to generate *in situ* probes are listed in Supplementary Table 3.
841 *Bottom*: Magnified image of *jhamt* and *nanos* mRNA within the boxed area. **c** *Top*: schematic of
842 the JH reporter transgene (JHRE-GFP) in which eight copies of the JH Response Element from
843 the *early trypsin* gene from *A. aegypti* was placed upstream of eGFP (See Materials and
844 Methods for construct design). *Bottom*: Induction of *kr-h1* mRNA, a known JH transcriptional
845 target, and *GFP* mRNA. deltaCt was calculated relative to the average Ct of two housekeeping
846 genes, *DCTN5-p25* and *Und*, and fold change was calculated by for whole second instar larvae
847 fed cornmeal food containing 1.6µg/mg of the JH analogue, methoprene normalized to age and
848 genotype-matched larvae fed ethanol. Animals were fed methoprene or ethanol as a control for
849 24 hours prior to RNA isolation. Bars and error bars represent average fold change and
850 standard deviation from three biological replicates, each consisting of ten second instar larvae.
851 **d** *Left:* Dorsal/Ventral (d/v) images of Stage 10 *JHRE-GFP* embryos that are wild type or mutant
852 for Met and Gce. Right: Magnified images of the boxed area. **e** *Left:* d/v view images of a Stage
853 11 *JHRE-GFP* embryo stained for GFP (green), Vasa (magenta) protein, and DNA using DAPI
854 (gray). *Right*: d/v view of a Stage 11 JHRE-GFP embryo. GFP staining only is shown below
855 each merged image. For all images, genotypes are shown in the top left corner, embryo
856 orientation in the top right corner. All embryo images are maximum projections of two to three
857 2µm confocal slices and scale bars represent 25µm in all images.

858

859

860

861

862

863

864

865

866

867

868 **Figure 2: The key JH biosynthesis enzyme, Jhamt, facilitates germ cell migration to the**
869 **somatic gonad. a** Schematic of the JH biosynthetic pathway from Acetyl co-A upstream of
870 Hmgcr activity to final steps involving Jhamt methyl transferase activity. **b** Schematic of the
871 *jhamt* locus noting where the CRISPR-mediated editing created 15 stable animal lines
872 containing indels to generate premature stop codons (denoted by Stop) within the
873 methyltransferase domain (shown in green). Light gray denotes 5' and 3' UTR. **c** Titers of two
874 JHs, JH III and JH bisepoxide (JH B3) in hemolymph of third instar *Drosophila* larvae measured
875 by quantitative mass spectrometry using deuterated standards. Each dot represents a biological
876 replicate of hemolymph bled from 25 larvae. For titers, w^{-}, *Sp/CyO,ft-lacZ* was used as a wild
877 type strain as the CRiSPR-induced alleles in a w^{-} background were initially crossed into this
878 background. **d** Fecundity of young females. Each dot represents the average number of eggs
879 laid per female from cohorts of 10-12 females in a 24-hour period three- and four-days post
880 eclosion. To avoid male reproductive effects, all virgin females were mated to wild type (w^{1118})
881 males. For **c-d**, bars and whiskers represent mean +/- standard deviation and statistical
882 significance was tested by unpaired student t test. **e** Dorsal/Ventral (d/v) view images of Stage
883 14 *Drosophila* embryos stained for Vasa (magenta) and DNA (DAPI, gray). Zygotic genotypes
884 are noted in the top left corner. To yield $jhamt^{-/-}$ embryos, with heteroallelic combinations of
885 independently-derived indels, $jhamt^{8F1}$*/CyO,ftz-lacZ* females were mated to $jhamt^{12F1}$*/CyO,ftz-*
886 *lacZ*. To generate $jhamt^{-/Def}$, $jhamt^{8F1}$*/CyO,ftz-lacZ* animals were mated to *Df(2L)BSC781/CyO,*
887 *ft-lacZ* animals. Gonads are circled with a yellow dashed circle. Arrowheads highlight
888 extragonadal germ cells. All embryo images are maximum projections of two to three 2µm
889 confocal slices and scale bars represent 25µm. **f** Quantification of extragonadal PGCs in Stage
890 14-16 embryos. Each dot represents one embryo. To the right of the dashed line, $jhamt^{+/-}$ virgin
891 females were either crossed to w^{1118} or $hmgcr^{+/-}$ males and unbalanced Stage 14+ progeny
892 were scored. *jhamt* and *hmgcr* alleles used are described in Supplemental Table 1. **g**
893 Quantification of the number of germ cells remaining outside the gonad of Stage 14-16 embryos
894 when Hmgcr is ectopically expressed in the nervous system using *Elav-GAL4* and *UAS-hmgcr*.
895 For panels **d-g**, bars and whiskers represent median +/- interquartile range (IQR), statistical
896 significance was tested by Mann-Whitney U test, and w^{1118} was used as a reference strain.
897
898
899
900
901

902 **Figure 3: Juvenile Hormone is sufficient for germ cell migration**. **a** Dorsal/Ventral (d/v) view
903 images of Stage 14 embryos stained for Vasa (magenta) and Elav (green). Genotypes are
904 noted in the top left corner of each image. Arrowheads highlight germ cells in contact with Elav-
905 positive central nervous system. Scale bars represent 25μm images. **b** Quantification of the
906 number of PGCs in Stage 14-16 embryos contacting Elav-positive cells upon ectopic expression
907 of either *Hmgcr* or *Jhamt* using the *Elav-GAL4* driver. Bar and whiskers represent mean +/-
908 standard deviation and statistical significance was tested by unpaired t-test. **c** *Top Left*: Scatter
909 plots from FACS of GFP-positive PGCs from *nos-moesin::GFP* transgenic embryos. Region 1
910 (R1) denotes collection cutoff. *Top Right*: Image of isolated GFP-positive germ cells. *Bottom*:
911 Schematic of *in vitro* transwell assay in which FACS-enriched PGCs are placed on a 10μm filter
912 above either serum-free media conditioned with Kc167 cells as a positive control, serum free
913 unconditioned media as a negative control, or experimental conditions such as serum-free
914 media with JH III. The number of PGCs that translocated to the bottom well was quantified
915 manually after 1.5 hours. **d** Quantification of Specific PGC migration, which is the percentage of
916 experimental PGCs that translocate relative to positive (serum-free Kc167-conditioned media)
917 and negative (serum-free media) controls to allow for comparison across biological replicates
918 done on different days. See Materials and Methods for further details on assay design and
919 derivation of percent specific migration. Numbers shown in white within each *jhamt* knockdown
920 bar represents the Fold Change (FC) of *jhamt* mRNA at the time conditioned media was
921 collected. Bar height represents mean and error bars represent standard deviation from two to
922 four biological replicates and statistical significance was tested by unpaired t-test. **e**
923 Quantification of specific migration in transwell assays using isolated PGCs placed above
924 serum-free media containing various concentrations of commercially available JH III (green
925 bars) or 20-hydroxyecdysone (20E, magenta bars) with 1% BSA as a non-specific carrier
926 protein. Bars represent means and error bars represent standard deviation from three biological
927 replicates, which were each obtained by averaging two to three technical replicates. **f**
928 Percentage specific migration wherein isolated PGCs were placed across either serum-free
929 media conditioned (gray), serum-free media with 1% BSA (black) and either JH III (dark green,
930 2.5μM) or the JH analogue, methoprene, (light green, 2.5μm) with 1% BSA as a non-specific
931 carrier protein. Bars represent means and error bars represent standard deviation from at two
932 biological replicates, which were each obtained by averaging two to three technical replicates.
933
934
935

936 **Figure 4: JHs impact germ cell migration through cytoplasmic signaling a** Schematic of
937 the nuclear and cytoplasmic proteins implicated in cellular responses to extracellular JH. **b**
938 Lateral view images of Stage 14 embryos stained for Vasa (magenta) and DAPI (gray).
939 Maternal and zygotic genotype are noted in the top left corner. To generate maternal and
940 zygotic mutant embryos, mutant $met^{1/27}$, $gce^{Mi/2.5k}$ mothers were crossed to met^{1},gce^{Mi}/*Y* males.
941 Arrowheads point to extragonadal germ cells. **c** Quantification of extragonadal PGCs from
942 Stage 14-16 embryos. The maternal and paternal genotypes in relation to *met, gce* are noted as
943 + or -. Arrowheads highlight extragonadal germ cells. To yield embryos in which maternal
944 contributions of Met and Gce were mutant, $met^{1/27}$, $gce^{Mi/2.5k}$ females were used. For maternal
945 mutant and zygotic mutant embryos, $met^{1/27}$, $gce^{Mi/2.5k}$ females were crossed to met^{1},gce^{Mi}/*Y*
946 males. For maternal mutant, zygotic wildtype embryos, $met^{1/27}$, $gce^{Mi/2.5k}$ females were crossed
947 to w^{1118} males. For maternal wildtye and zygotic mutant embryos, met^{27}, $gce^{2.5k}$/*Fm7a* females
948 were crossed to met^{1},gce^{Mi}/*Y* males. **d** *Top panels*: schematic of genetic suppression
949 experiment. In otherwise wild type embryos, ectopic expression of Hmgcr in the endoderm
950 (green) using the *48Y-GAL4; UASt-Hmgcr* will trap ~75% of PGCs (pink) in the gut (*left*
951 *schematic*). To test the role of Met and Gce downstream of Hmgcr, we crossed $met^{1/27}$, $gce^{Mi/2.5k}$
952 females to *48Y-GAL4; UASt-Hmgcr* males (*right schematic*) and measured how many PGCs
953 remained trapped in the endoderm after PGC colonization of the gonad is complete. *Bottom*
954 *panels*: Lateral view images of Stage 14 embryos stained for Vasa (magenta), the endodermal
955 marker, Hnt (green) and the DNA stain, DAPI (gray). Bold **M**: designates the maternal genotype
956 that PGCs primarily rely on when exiting the endoderm. Females mutant for met and gce were
957 heteroallelic $met^{1/27}$, $gce^{Mi/2.5k}$. Bold **P**: designates the paternal genotype in which *Hmgcr* is
958 ectopically expressed in the endoderm using the *48Y-GAL4* driver. White brackets indicate
959 germ cells that remain in gut. **e** Quantification of the percentage of PGCs remaining in the gut in
960 Stage 14+ embryos upon expression of *UAS-Hmgcr* using the *48Y-GAL4* driver. For panels B-
961 E, the wild type reference strain was obtained by crossing w^{1118} to OregonR, as *met* and *gce*
962 alleles used were generated from both of these genetic backgrounds (**Supp Table 1**). **f**
963 Quantification of specific *in vitro* migration when isolated PGCs were treated with 1μM
964 flavopiridol to inhibit transcription (Txn) or vehicle control for 30 minutes before being placed in
965 the transwell membrane across serum-free media alone (black) or serum-free media
966 conditioned with Kc167 (gray) or containing 5μM JH III (green). Bars represent means and error
967 bars represent standard deviation from two biological replicates, which were each obtained by
968 averaging two technical replicates. **g** *Left*: d/v view images of Stage 14 embryos stained for
969 Vasa (magenta) and DAPI (gray). Maternal and zygotic genotype is noted in the top left corner.

970 To generate embryos maternally and zygotically depleted of Plc21c, *plc21c*$^{Mi/Df(2L)BSC106}$ females
971 were crossed to *plc21c*^{Mi}*/CyO,ft-lacZ* males. Detailed descriptions of the mutant alleles are
972 described in Supplemental Table 1. Wild type reference strain was w^{1118}. Arrowheads point to
973 extragonadal germ cells. **h** Quantification of extragonadal PGCs in Stage 14-16 embryos.
974 Maternal and zygotic genotypes are noted below each column. **i** *Top*: Schematic of experiment
975 to test whether the maternal loss of Plc21c suppresses the ability of ectopic endodermal Hmgcr
976 (green) to trap PGCs (pink) in the gut. *Bottom*: Dorsal/Ventral view images of Stage 14 embryos
977 stained for Vasa (magenta), the endodermal marker, Hnt (green) and the DNA stain, DAPI
978 (gray). Bold **M**: designates the maternal genotype that PGCs primarily rely on when exiting the
979 endoderm. Maternal *plc21c* mutant genotype was heteroallelic *plc21c*$^{Mi/Df(2L)BSC106}$. Bold **P**:
980 designates the paternal genotype in which Hmgcr is ectopically expressed in the endoderm
981 using the *48Y-GAL4* driver. White brackets indicate germ cells that remain in gut. **j**
982 Quantification of the percentage of PGCs remaining in the gut in Stage 14+ embryos when
983 Hmgcr was ectopically expressed in the developing gut using *48Y-GAL4; UASt-Hmgcr*
984 transgenes. Wild type control is w^{1118}. For **c**, **e**, **h and j**, each dot represents one embryo. Bars
985 and whiskers represent median +/- IQR and statistical significance was assessed by Mann-
986 Whitney U test. ns- not significant. Dashed yellow circle highlight the gonad and scale bars
987 represent 25μm in all images.
988
989
990
991
992
993
994
995
996
997
998
999
1000
1001
1002

1003 **Figure 5: Tests of conserved impact of, and model for, isoprenoids in germ cell**
1004 **migration. a** Quantification of specific *in vitro* migration wherein isolated *Drosophila* PGCs are
1005 placed in a transwell migration system across Kc167-conditioned media (gray), serum-free
1006 media (black), JH III (green, 5μM), all trans retinoic acid (ATRA, dark blue, 5μM) or 9-cis RA
1007 (light blue 5μM). **b** Quantification of specific *in vitro* migration wherein mouse PGCs were FACS-
1008 enriched from trunk tissues dissected from E10.5 *Oct4-GFP* embryos and placed across two
1009 positive controls: Fetal Bovine Serum (FBS) or CXCL12 (50 ng/mL) (gray), serum-free media as
1010 a negative control (black) or ATRA (dark blue, 1μM) or 9cis-RA (light blue, 1μM). For **A** and **B**,
1011 bars and error bars represent mean +/- standard deviation from at least two biological
1012 replicates, which were obtained by averaging two to three technical replicates. **c** Schematic of
1013 model for how the bioactive isoprenoids, such as JH, ensure migrating PGCs (pink) colonize the
1014 somatic gonad (green). Also included is a model for what is required within PGCs to respond to
1015 JH. Purple cylinders at the plasma membrane represent an unknown JH receptor thought to link
1016 JH to Plc21c activation. Signaling from Plc21c to JH nuclear receptors (JHNR, yellow circle),
1017 Met or Gce remains to be determined but a role for transcription is not required. Model JH
1018 transcriptional target is shown within the blue nucleus, wherein the target gene is shown as a
1019 gray rectangle, the JHNR is a yellow circle and the JHNR co-factor, Taiman is shown as a red
1020 circle.
1021
1022
1023
1024
1025
1026
1027
1028
1029
1030
1031
1032
1033
1034
1035
1036

1037 **Supplemental Data for Figure 1 a** Sequence of the JH response element (JHRE) from the
1038 *early trypsin* gene of *A. aegypti* that contains the JH nuclear receptor (JHNR) binding motif
1039 highlighted in bold[24]. The six base pair wild type JHRE sequence is on top and the JHRE in
1040 which the JHNR-binding motif was mutated is on the bottom. Eight copies of each sequence
1041 were provided by Marek Jindra[23] and placed upstream of *eGFP*. **b** Dorsal/ventral (d/v) view of
1042 Stage 14 JHRE Mut8x-GFP embryo stained for GFP (green) and the hemocyte marker, Fascin
1043 (gray). Right panel is the same image but with the Fascin signal alone in grayscale. **c** Lateral
1044 view of embryos stained for Vasa (magenta), GFP (green) and DAPI (gray). Genotype is noted
1045 above each early Stage 12 and Stage 14 pair. To the right of each whole-embryo image is the
1046 area within the white, dashed box magnified. Scale bars represent 25μm in all images.
1047
1048 **Supplemental Data for Figure 2** Nature of the small deletions in *jhamt* created by CRISPR-
1049 mediated cutting. Seven founders generated fifteen lines which possessed small insertions or
1050 deletions at the cut site that created premature stop codons at the beginning of methyl
1051 transferase domain of *jhamt* (amino acids 40-137). Class 1 lines (12F1, 12F2) cause a
1052 premature stop codon at amino acid 46, while Class II mutations (1F1, 1F2, 4F1, 4F3, 6F2, 6F3,
1053 7F2, 7F3, 8F1, 8F2, 12F3, 14M2, 14M3) cause a premature stop codon at amino acid 54.
1054
1055 **Supplemental Data for Figure 3 a** *Left:* Quantification of the number of PGCs in Stage 14-16
1056 embryos that remained in the gut upon ectopic expression of either *Hmgcr* or *jhamt* using the
1057 *48Y-GAL4* driver. *Right:* Quantification of the number of germ cell in Stage 14-16 embyros that
1058 contact Zfh-1-positive cells upon the expression of either *Hmgcr* or *jhamt* using the *twist(twi)-*
1059 *GAL4* and *24B-GAL4* drivers. Each dot represents one embryo. Bars and whiskers represent
1060 median +/- IQR and statistical significance was analyzed by the Mann-Whitney U test. **b**
1061 Quantification of the number of Kc167 cells that were used to condition serum-free media after
1062 *jhamt* mRNA was knocked down relative to the number of Kc167cells in the transfection control.
1063 Bars and error bars represent mean +/- standard deviation from two biological replicates. **c**
1064 Quantification of the fold change in mRNAs in Schneider 2 (S2) cells upon incubation with
1065 varying concentrations of 20-Ecdysone (20-E) or JH III for six hours prior to mRNA isolation.
1066 mRNAs from two verified ecdysone-responsive genes were measured: *Eip74b* (lighter purple)
1067 and *Eip75* (darker purple) and one JH-responsive gene was measured, *Kr-h1* (green) and
1068 normalized to the housekeeping gene, *DCTN2-p50*. Error bars represent standard deviation
1069 from two biological replicates.
1070

1071 **Supplemental Data for Figure 4 a** Schematics of *met* and *gce* loci indicating the mutations that
1072 were recombined to yield met^{1}, gce^{Mi} alleles. **b** Quantification of fold change of *gce* and *Kr-h1*
1073 mRNAs in *met, gce* mutant one-day old adult females relative to wildtype control animals.
1074 deltaCt was calculated relative to the average Ct of two housekeeping genes, *DCTN5-p25* and
1075 *Und*. Shown are females homoallelic for the newly recombined mutant alleles met^{1}, gce^{Mi} (dark
1076 blue) and heteroallelic combination with existing or met^{27}, $gce^{2.5k}$ alleles (light blue). Bars and
1077 error bars represent mean +/- standard deviation from three biological replicates of five females
1078 each. **c** Fecundity of young females. Each dot represents the average number of eggs laid in a
1079 24-hour period from a cohort of 10-12 three- and four-days post eclosion females per biological
1080 replicate. To avoid male reproductive effects, all virgin females were mated to wild type, w^{1118},
1081 males. Bars and whiskers represent mean +/- standard deviation, which statistical significance
1082 analyzed by unpaired t-test. **d** Images of *Drosophila* PGCs enriched by FACS and stained for
1083 Vasa (magenta), RNA Pol II, Ser5p (green), RNA Pol II, Ser2p (yellow) and DAPI (gray). Bottom
1084 panel shows a germ cell treated with 1μM Flavopiridol for 3 hours. Scale bars represent 5μm. **e**
1085 JH titers in hemolymph of second instar larvae measured by quantitative mass spectrometry in
1086 wild type and met^{1}, gce^{Mi} mutant larvae. Each dot represents a biological replicate of
1087 hemolymph from 25 larvae. Error bars represent standard deviation and p values are from
1088 unpaired t-tests.
1089
1090 **Supplemental Data for Figure 5 a** Scatter plots from FACS of GFP-positive PGCs enriched
1091 from trunks of E10.5 mouse embryos carrying the *Oct4ΔPE::GFP* reporter. The number inside
1092 the gate lines denotes the percentage of collected events in a typical biological replicate. **b**
1093 Quantification of the percent change in the number of mouse germ cells before and two hours
1094 after application of 1μm ATRA or 9cis-RA. Two hours was chosen because this is the duration
1095 of the *in vitro* migration assay. Graphed is the mean and standard deviation from three
1096 biological replicated. Each dot represents the averaged technical replicates of each biological
1097 replicate.
1098
1099
1100
1101
1102
1103
1104
1105
1106

1107 **References**
1108

1109 1. Richardson, B.E. & Lehmann, R. Mechanisms guiding primordial germ cell migration:
1110 strategies from different organisms. *Nat Rev Mol Cell Biol* **11**, 37-49 (2010).
1111 2. Saitou, M., Kagiwada, S. & Kurimoto, K. Epigenetic reprogramming in mouse pre-
1112 implantation development and primordial germ cells. *Development* **139**, 15-31 (2012).
1113 3. Siddiqui, N.U. *et al.* Genome-wide analysis of the maternal-to-zygotic transition in
1114 Drosophila primordial germ cells. *Genome Biol* **13**, R11 (2012).
1115 4. Slaidina, M. & Lehmann, R. Quantitative Differences in a Single Maternal Factor
1116 Determine Survival Probabilities among Drosophila Germ Cells. *Current biology : CB* **27**,
1117 291-297 (2017).
1118 5. Nicholls, P.K. *et al.* Mammalian germ cells are determined after PGC colonization of the
1119 nascent gonad. *Proceedings of the National Academy of Sciences of the United States of*
1120 *America* **116**, 25677-25687 (2019).
1121 6. Olmstead, A.W. & Leblanc, G.A. Juvenoid hormone methyl farnesoate is a sex
1122 determinant in the crustacean Daphnia magna. *J Exp Zool* **293**, 736-739 (2002).
1123 7. Bowles, J. *et al.* Retinoid signaling determines germ cell fate in mice. *Science* **312**, 596-
1124 600 (2006).
1125 8. Koubova, J. *et al.* Retinoic acid regulates sex-specific timing of meiotic initiation in mice.
1126 *Proceedings of the National Academy of Sciences of the United States of America* **103**,
1127 2474-2479 (2006).
1128 9. Bowles, J. *et al.* Retinoic Acid Antagonizes Testis Development in Mice. *Cell Rep* **24**,
1129 1330-1341 (2018).
1130 10. Miyauchi, H. *et al.* Bone morphogenetic protein and retinoic acid synergistically specify
1131 female germ-cell fate in mice. *EMBO J* **36**, 3100-3119 (2017).
1132 11. Chassot, A.A. *et al.* Retinoic acid synthesis by ALDH1A proteins is dispensable for meiosis
1133 initiation in the mouse fetal ovary. *Sci Adv* **6**, eaaz1261 (2020).
1134 12. Vernet, N. *et al.* Meiosis occurs normally in the fetal ovary of mice lacking all retinoic
1135 acid receptors. *Sci Adv* **6** (2020).
1136 13. Bowles, J. *et al.* ALDH1A1 provides a source of meiosis-inducing retinoic acid in mouse
1137 fetal ovaries. *Nat Commun* **7**, 10845 (2016).
1138 14. Kumar, S. *et al.* Sex-specific timing of meiotic initiation is regulated by Cyp26b1
1139 independent of retinoic acid signalling. *Nat Commun* **2**, 151 (2011).
1140 15. Minkina, A. *et al.* Retinoic acid signaling is dispensable for somatic development and
1141 function in the mammalian ovary. *Developmental biology* **424**, 208-220 (2017).
1142 16. Hartfelder, K. Insect juvenile hormone: from "status quo" to high society. *Braz J Med*
1143 *Biol Res* **33**, 157-177 (2000).
1144 17. Casper, A.L. & Van Doren, M. The establishment of sexual identity in the Drosophila
1145 germline. *Development* **136**, 3821-3830 (2009).
1146 18. Niederreither, K., Fraulob, V., Garnier, J.M., Chambon, P. & Dolle, P. Differential
1147 expression of retinoic acid-synthesizing (RALDH) enzymes during fetal development and
1148 organ differentiation in the mouse. *Mech Dev* **110**, 165-171 (2002).
1149 19. Niwa, R. *et al.* Juvenile hormone acid O-methyltransferase in Drosophila melanogaster.
1150 *Insect Biochem Mol Biol* **38**, 714-720 (2008).

1151 20. Van Doren, M., Broihier, H.T., Moore, L.A. & Lehmann, R. HMG-CoA reductase guides
1152 migrating primordial germ cells. *Nature* **396**, 466-469 (1998).
1153 21. Riddiford, L.M. Rhodnius, Golden Oil, and Met: A History of Juvenile Hormone Research.
1154 *Front Cell Dev Biol* **8**, 679 (2020).
1155 22. Sanchez-Higueras, C. & Hombria, J.C. Precise long-range migration results from short-
1156 range stepwise migration during ring gland organogenesis. *Developmental biology* **414**,
1157 45-57 (2016).
1158 23. Jindra, M., Uhlirova, M., Charles, J.P., Smykal, V. & Hill, R.J. Genetic Evidence for
1159 Function of the bHLH-PAS Protein Gce/Met As a Juvenile Hormone Receptor. *PLoS Genet*
1160 **11**, e1005394 (2015).
1161 24. Noriega, F.G., Shah, D.K. & Wells, M.A. Juvenile hormone controls early trypsin gene
1162 transcription in the midgut of Aedes aegypti. *Insect Mol Biol* **6**, 63-66 (1997).
1163 25. Ramirez, C.E., Nouzova, M., Michalkova, V., Fernandez-Lima, F. & Noriega, F.G. Common
1164 structural features facilitate the simultaneous identification and quantification of the
1165 five most common juvenile hormones by liquid chromatography-tandem mass
1166 spectrometry. *Insect Biochem Mol Biol* **116**, 103287 (2020).
1167 26. Wen, D. *et al.* Methyl farnesoate plays a dual role in regulating Drosophila
1168 metamorphosis. *PLoS Genet* **11**, e1005038 (2015).
1169 27. Kenwrick, K., Mukherjee, A. & Renault, A.D. Hmgcr promotes a long-range signal to
1170 attract Drosophila germ cells independently of Hedgehog. *J Cell Sci* **132** (2019).
1171 28. Goldstein, J.L. & Brown, M.S. Regulation of the mevalonate pathway. *Nature* **343**, 425-
1172 430 (1990).
1173 29. Ricardo, S. & Lehmann, R. An ABC transporter controls export of a Drosophila germ cell
1174 attractant. *Science* **323**, 943-946 (2009).
1175 30. Bai, J., Uehara, Y. & Montell, D.J. Regulation of invasive cell behavior by taiman, a
1176 Drosophila protein related to AIB1, a steroid receptor coactivator amplified in breast
1177 cancer. *Cell* **103**, 1047-1058 (2000).
1178 31. Banisch, T.U. *et al.* A transitory signaling center controls timing of primordial germ cell
1179 differentiation. *Dev Cell* **56**, 1742-1755 e1744 (2021).
1180 32. Abdou, M.A. *et al.* Drosophila Met and Gce are partially redundant in transducing
1181 juvenile hormone action. *Insect Biochem Mol Biol* **41**, 938-945 (2011).
1182 33. Wilson, T.G., Wang, S., Beno, M. & Farkas, R. Wide mutational spectrum of a gene
1183 involved in hormone action and insecticide resistance in Drosophila melanogaster. *Mol*
1184 *Genet Genomics* **276**, 294-303 (2006).
1185 34. Bensaude, O. Inhibiting eukaryotic transcription: Which compound to choose? How to
1186 evaluate its activity? *Transcription* **2**, 103-108 (2011).
1187 35. Yamamoto, K., Chadarevian, A. & Pellegrini, M. Juvenile hormone action mediated in
1188 male accessory glands of Drosophila by calcium and kinase C. *Science* **239**, 916-919
1189 (1988).
1190 36. Pszczolkowski, M.A., Peterson, A., Srinivasan, A. & Ramaswamy, S.B. Pharmacological
1191 analysis of ovarial patency in Heliothis virescens. *J Insect Physiol* **51**, 445-453 (2005).
1192 37. Pszczolkowski, M.A., Olson, E., Rhine, C. & Ramaswamy, S.B. Role for calcium in the
1193 development of ovarial patency in Heliothis virescens. *J Insect Physiol* **54**, 358-366
1194 (2008).

1195 38. Liu, P., Peng, H.J. & Zhu, J. Juvenile hormone-activated phospholipase C pathway
1196 enhances transcriptional activation by the methoprene-tolerant protein. *Proceedings of*
1197 *the National Academy of Sciences of the United States of America* **112**, E1871-1879
1198 (2015).
1199 39. Ojani, R., Liu, P., Fu, X. & Zhu, J. Protein kinase C modulates transcriptional activation by
1200 the juvenile hormone receptor methoprene-tolerant. *Insect Biochem Mol Biol* **70**, 44-52
1201 (2016).
1202 40. Cai, M.J. *et al.* Juvenile hormone prevents 20-hydroxyecdysone-induced metamorphosis
1203 by regulating the phosphorylation of a newly identified broad protein. *The Journal of*
1204 *biological chemistry* **289**, 26630-26641 (2014).
1205 41. Jing, Y.P., An, H., Zhang, S., Wang, N. & Zhou, S. Protein kinase C mediates juvenile
1206 hormone-dependent phosphorylation of Na(+)/K(+)-ATPase to induce ovarian follicular
1207 patency for yolk protein uptake. *The Journal of biological chemistry* **293**, 20112-20122
1208 (2018).
1209 42. Moore, L.A., Broihier, H.T., Van Doren, M., Lunsford, L.B. & Lehmann, R. Identification of
1210 genes controlling germ cell migration and embryonic gonad formation in Drosophila.
1211 *Development* **125**, 667-678 (1998).
1212 43. Harmon, M.A., Boehm, M.F., Heyman, R.A. & Mangelsdorf, D.J. Activation of mammalian
1213 retinoid X receptors by the insect growth regulator methoprene. *Proceedings of the*
1214 *National Academy of Sciences of the United States of America* **92**, 6157-6160 (1995).
1215 44. Knaut, H., Werz, C., Geisler, R., Nusslein-Volhard, C. & Tubingen Screen, C. A zebrafish
1216 homologue of the chemokine receptor Cxcr4 is a germ-cell guidance receptor. *Nature*
1217 **421**, 279-282 (2003).
1218 45. Doitsidou, M. *et al.* Guidance of primordial germ cell migration by the chemokine SDF-1.
1219 *Cell* **111**, 647-659 (2002).
1220 46. Molyneaux, K.A. *et al.* The chemokine SDF1/CXCL12 and its receptor CXCR4 regulate
1221 mouse germ cell migration and survival. *Development* **130**, 4279-4286 (2003).
1222 47. Koshimizu, U., Watanabe, M. & Nakatsuji, N. Retinoic acid is a potent growth activator
1223 of mouse primordial germ cells in vitro. *Developmental biology* **168**, 683-685 (1995).
1224 48. Ashok, M., Turner, C. & Wilson, T.G. Insect juvenile hormone resistance gene homology
1225 with the bHLH-PAS family of transcriptional regulators. *Proceedings of the National*
1226 *Academy of Sciences of the United States of America* **95**, 2761-2766 (1998).
1227 49. Tomancak, P. *et al.* Systematic determination of patterns of gene expression during
1228 Drosophila embryogenesis. *Genome Biol* **3**, RESEARCH0088 (2002).
1229 50. Rahman, M.M., Franch-Marro, X., Maestro, J.L., Martin, D. & Casali, A. Local Juvenile
1230 Hormone activity regulates gut homeostasis and tumor growth in adult Drosophila. *Sci*
1231 *Rep* **7**, 11677 (2017).
1232 51. Luo, W. *et al.* Dual roles of juvenile hormone signaling during early oogenesis in
1233 Drosophila. *Insect Sci* **27**, 665-674 (2020).
1234 52. Weaver, L.N., Ma, T. & Drummond-Barbosa, D. Analysis of Gal4 Expression Patterns in
1235 Adult Drosophila Females. *G3 (Bethesda)* **10**, 4147-4158 (2020).
1236 53. Ilenchuk, T.T. & Davey, K.G. The Development of Responsiveness to Juvenile-Hormone
1237 in the Follicle Cells of Rhodnius-Prolixus. *Insect Biochemistry* **17**, 525-529 (1987).

1238 54. Yamamoto, K., Chadarevian, A. & Pellegrini, M. Juvenile-Hormone Action Mediated in
1239 Male Accessory-Glands of Drosophila by Calcium and Kinase-C. *Science* **239**, 916-919
1240 (1988).
1241 55. Sevala, V.L. & Davey, K.G. Action of Juvenile-Hormone on the Follicle Cells of Rhodnius-
1242 Prolixus - Evidence for a Novel Regulatory Mechanism Involving Protein Kinase-C.
1243 *Experientia* **45**, 355-356 (1989).
1244 56. Bai, H. & Palli, S.R. Identification of G protein-coupled receptors required for vitellogenin
1245 uptake into the oocytes of the red flour beetle, Tribolium castaneum. *Sci Rep* **6**, 27648
1246 (2016).
1247 57. Gancz, D., Lengil, T. & Gilboa, L. Coordinated regulation of niche and stem cell
1248 precursors by hormonal signaling. *PLoS biology* **9**, e1001202 (2011).
1249 58. Kozlova, T. & Thummel, C.S. Essential roles for ecdysone signaling during Drosophila
1250 mid-embryonic development. *Science* **301**, 1911-1914 (2003).
1251 59. Gilboa, L. & Lehmann, R. Soma-germline interactions coordinate homeostasis and
1252 growth in the Drosophila gonad. *Nature* **443**, 97-100 (2006).
1253 60. Arora, R. *et al.* Meiotic onset is reliant on spatial distribution but independent of germ
1254 cell number in the mouse ovary. *J Cell Sci* **129**, 2493-2499 (2016).
1255 61. Yao, H.H., DiNapoli, L. & Capel, B. Meiotic germ cells antagonize mesonephric cell
1256 migration and testis cord formation in mouse gonads. *Development* **130**, 5895-5902
1257 (2003).
1258 62. Iwata, M. *et al.* Retinoic acid imprints gut-homing specificity on T cells. *Immunity* **21**,
1259 527-538 (2004).
1260 63. Kim, M.H., Taparowsky, E.J. & Kim, C.H. Retinoic Acid Differentially Regulates the
1261 Migration of Innate Lymphoid Cell Subsets to the Gut. *Immunity* **43**, 107-119 (2015).
1262 64. Al Tanoury, Z., Piskunov, A. & Rochette-Egly, C. Vitamin A and retinoid signaling:
1263 genomic and nongenomic effects. *J Lipid Res* **54**, 1761-1775 (2013).
1264 65. Rand, C.D., Spencer, G.E. & Carlone, R.L. Retinoic acid as a chemoattractant for cultured
1265 embryonic spinal cord neurons of the African Clawed Frog, Xenopus laevis. *Can J Zool*
1266 **95**, 653-661 (2017).
1267 66. Farrar, N.R., Dmetrichuk, J.M., Carlone, R.L. & Spencer, G.E. A novel, nongenomic
1268 mechanism underlies retinoic acid-induced growth cone turning. *J Neurosci* **29**, 14136-
1269 14142 (2009).
1270 67. Vesprini, N.D., Dawson, T.F., Yuan, Y., Bruce, D. & Spencer, G.E. Retinoic acid affects
1271 calcium signaling in adult molluscan neurons. *J Neurophysiol* **113**, 172-181 (2015).
1272 68. Johnson, A., Nasser, T.I.N. & Spencer, G.E. Inhibition of Rho GTPases in Invertebrate
1273 Growth Cones Induces a Switch in Responsiveness to Retinoic Acid. *Biomolecules* **9**
1274 (2019).
1275 69. de Hoog, E., Lukewich, M.K. & Spencer, G.E. Retinoid receptor-based signaling plays a
1276 role in voltage-dependent inhibition of invertebrate voltage-gated Ca2+ channels.
1277 *Journal of Biological Chemistry* **294**, 10076-10093 (2019).
1278 70. Farini, D., La Sala, G., Tedesco, M. & De Felici, M. Chemoattractant action and molecular
1279 signaling pathways of Kit ligand on mouse primordial germ cells. *Developmental biology*
1280 **306**, 572-583 (2007).

1281 71. Laird, D.J., Altshuler-Keylin, S., Kissner, M.D., Zhou, X. & Anderson, K.V. Ror2 enhances
1282 polarity and directional migration of primordial germ cells. *PLoS Genet* **7**, e1002428
1283 (2011).
1284 72. Damdimopoulou, P., Chiang, C. & Flaws, J.A. Retinoic acid signaling in ovarian
1285 folliculogenesis and steroidogenesis. *Reprod Toxicol* **87**, 32-41 (2019).
1286 73. Santos, C.G., Humann, F.C. & Hartfelder, K. Juvenile hormone signaling in insect
1287 oogenesis. *Curr Opin Insect Sci* **31**, 43-48 (2019).
1288 74. Toyota, K. *et al.* Methyl farnesoate synthesis is necessary for the environmental sex
1289 determination in the water flea Daphnia pulex. *Journal of Insect Physiology* **80**, 22-30
1290 (2015).
1291 75. Vernet, N. *et al.* Meiosis occurs normally in the fetal ovary of mice lacking all retinoic
1292 acid receptors. *Science Advances* **6** (2020).
1293 76. Yoshimizu, T. *et al.* Germline-specific expression of the Oct-4/green fluorescent protein
1294 (GFP) transgene in mice. *Dev Growth Differ* **41**, 675-684 (1999).
1295 77. Restifo, L.L. & Wilson, T.G. A juvenile hormone agonist reveals distinct developmental
1296 pathways mediated by ecdysone-inducible broad complex transcription factors. *Dev*
1297 *Genet* **22**, 141-159 (1998).
1298 78. Lecuyer, E., Necakov, A.S., Caceres, L. & Krause, H.M. High-resolution fluorescent in situ
1299 hybridization of Drosophila embryos and tissues. *CSH Protoc* **2008**, pdb prot5019 (2008).
1300 79. Livak, K.J. & Schmittgen, T.D. Analysis of relative gene expression data using real-time
1301 quantitative PCR and the 2(-Delta Delta C(T)) Method. *Methods* **25**, 402-408 (2001).
1302 80. Celniker, S.E. *et al.* Unlocking the secrets of the genome. *Nature* **459**, 927-930 (2009).
1303 81. Barton, L.J. *et al.* Nuclear lamina dysfunction triggers a germline stem cell checkpoint.
1304 *Nat Commun* **9**, 3960 (2018).
1305 82. Wilson, T.G. & Fabian, J. A Drosophila melanogaster mutant resistant to a chemical
1306 analog of juvenile hormone. *Developmental biology* **118**, 190-201 (1986).
1307 83. Baumann, A.A. *et al.* Genetic tools to study juvenile hormone action in Drosophila. *Sci*
1308 *Rep* **7**, 2132 (2017).
1309 84. Venken, K.J. *et al.* MiMIC: a highly versatile transposon insertion resource for
1310 engineering Drosophila melanogaster genes. *Nat Methods* **8**, 737-743 (2011).
1311 85. Hu, Q., Velez-Aviles, A.N. & Wolfner, M.F. Drosophila Plc21C is involved in calcium wave
1312 propagation during egg activation. *MicroPubl Biol* **2020** (2020).
1313 86. Sano, H., Renault, A.D. & Lehmann, R. Control of lateral migration and germ cell
1314 elimination by the Drosophila melanogaster lipid phosphate phosphatases Wunen and
1315 Wunen 2. *The Journal of cell biology* **171**, 675-683 (2005).
1316

Figure 1
Juvenile hormone signaling is present during embryonic germ cell development

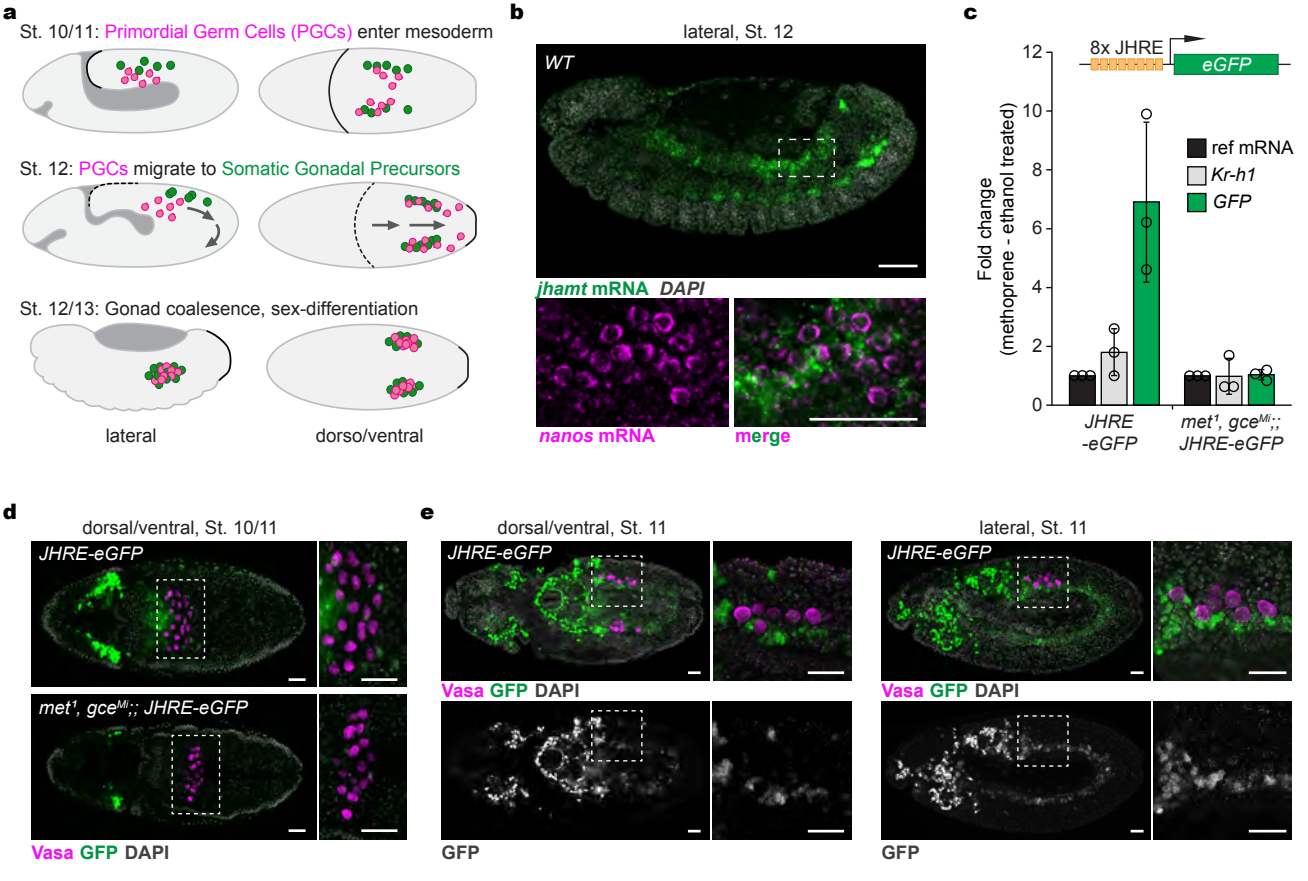

Figure 2

Key JH biosynthesis enzyme, Jhamt, facilitates germ cell migration to the somatic gonad

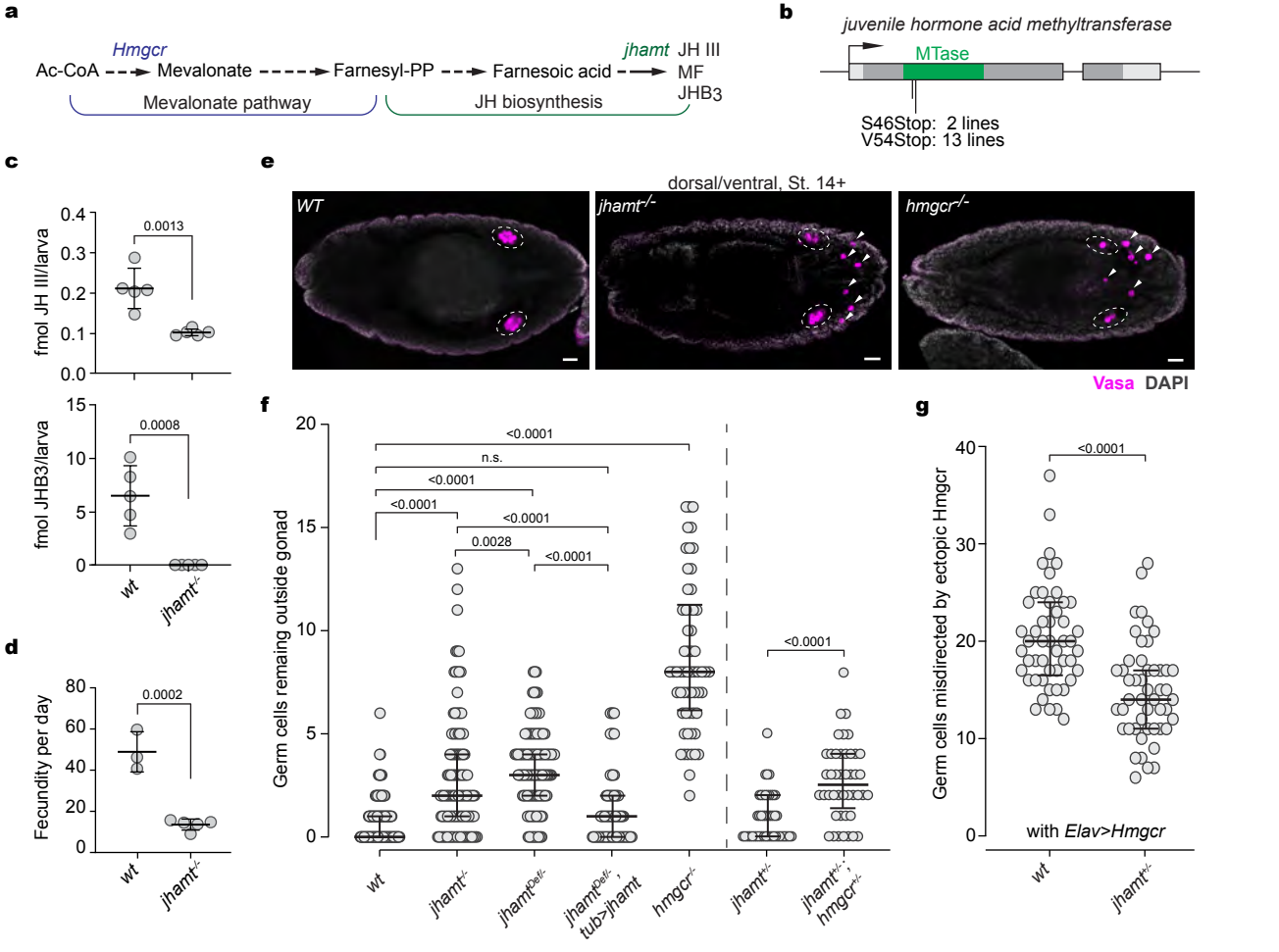

Figure 3
Juvenile hormone is sufficient for germ cell migration

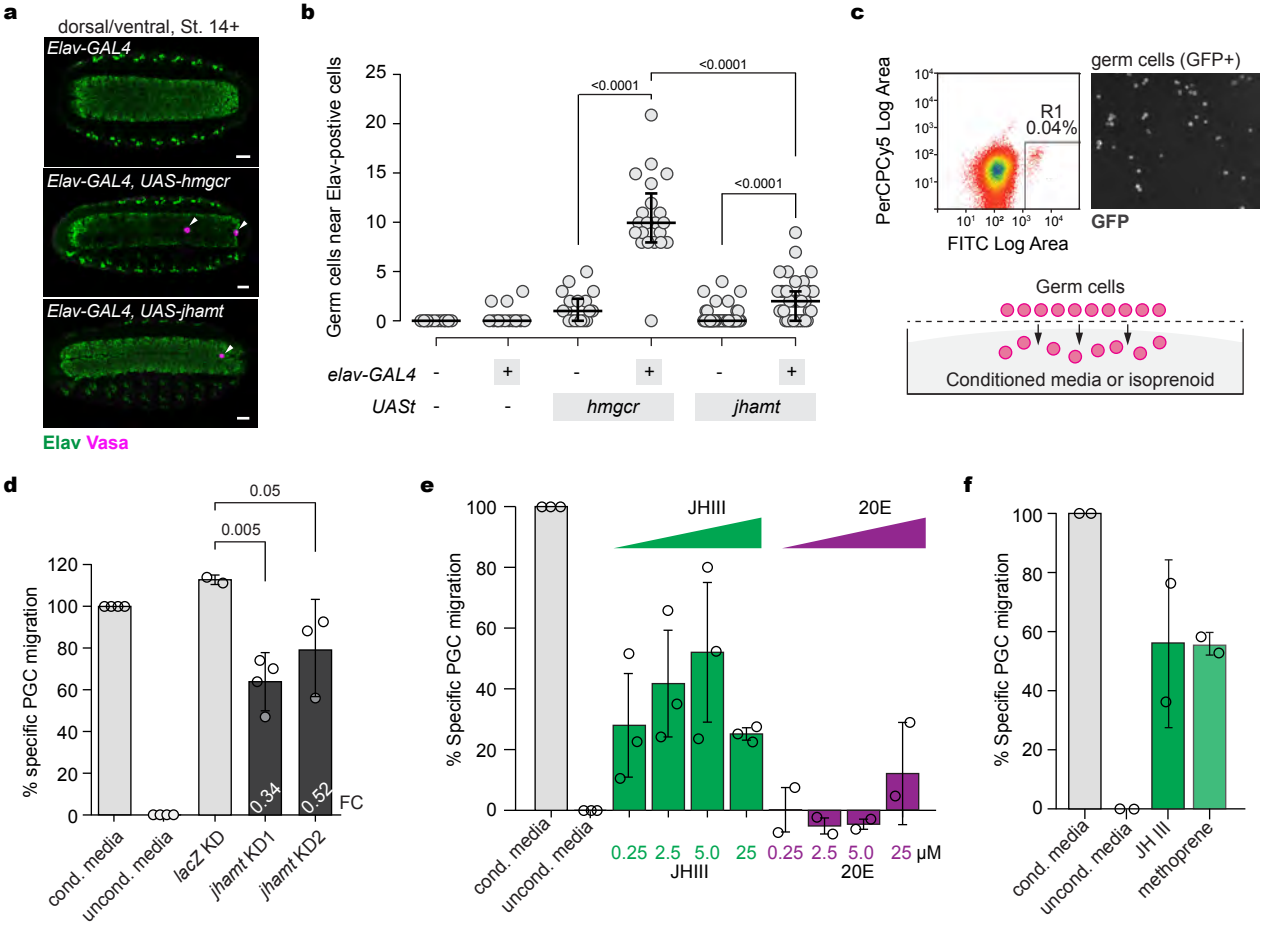

Figure 4
JHs impact germ cell migration through cytoplasmic signaling

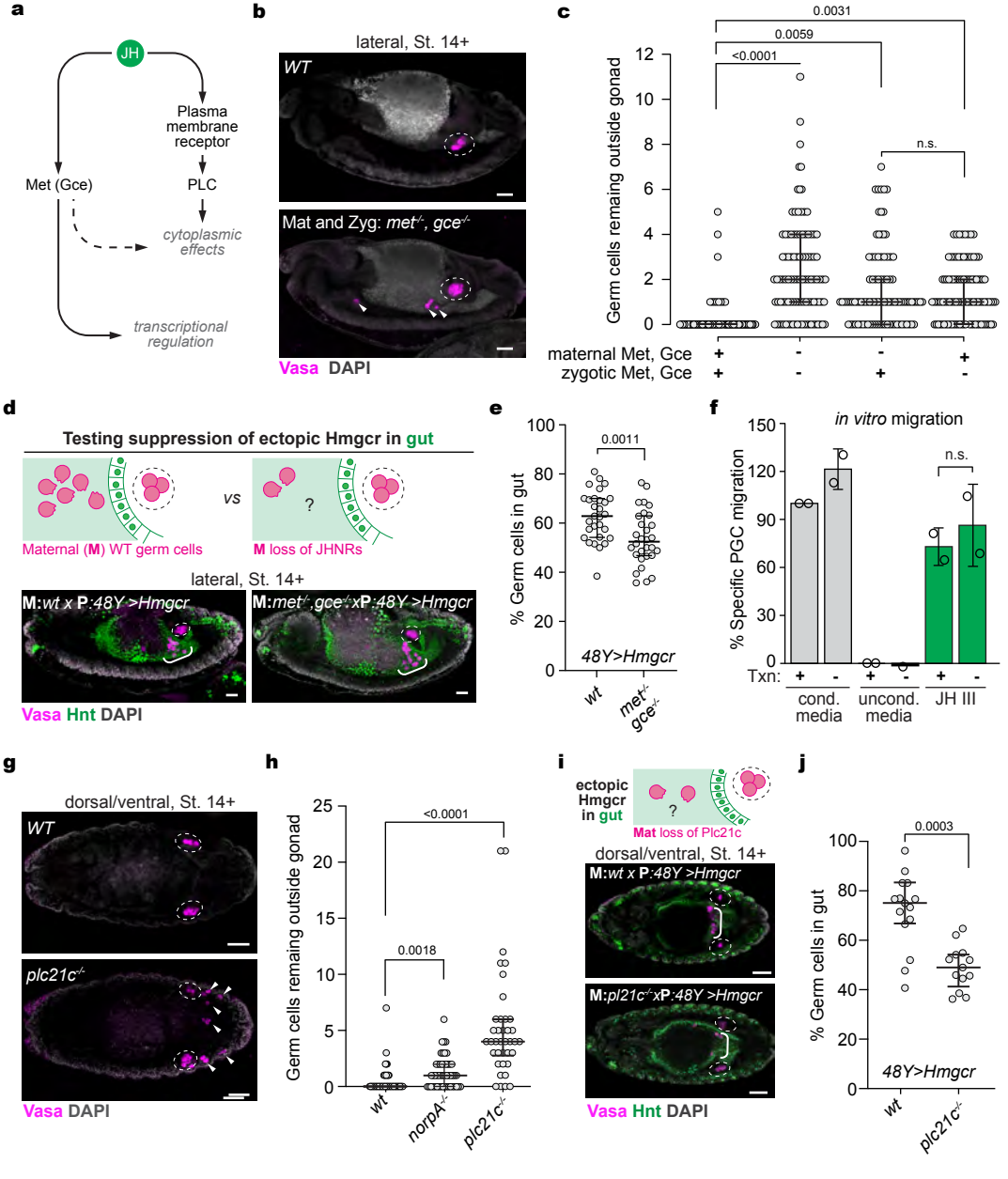

Figure 5

Tests of conservated impact of, and model for, isoprenoids in germ cell migration

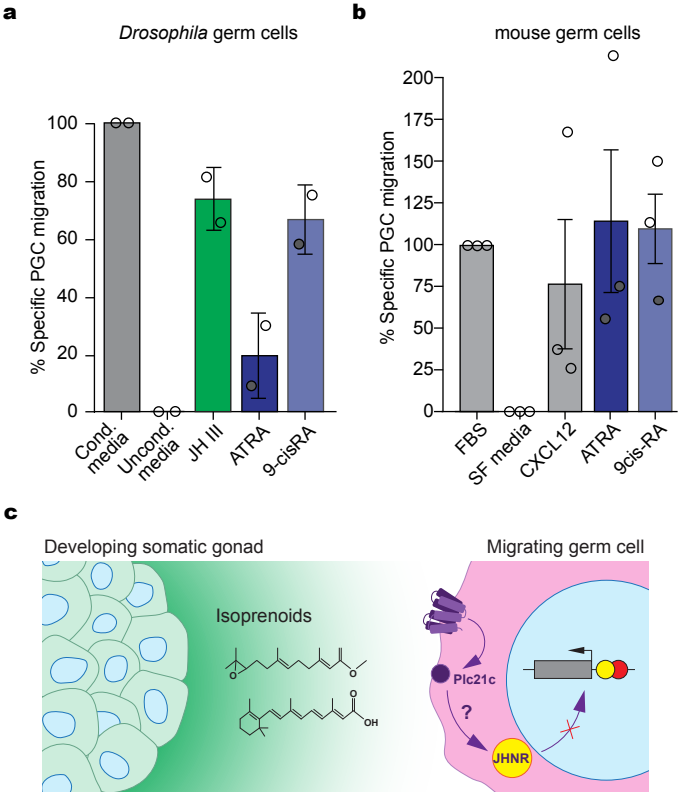

Supplementary Figure 1

a

```
JHRE Wt8x  -  5′ ccatccca CACGCG aagacgataaaacca 3′
JHRE Mut8x -  5′ ccatccca GTGCGC aagacgataaaacca 3′
```

b

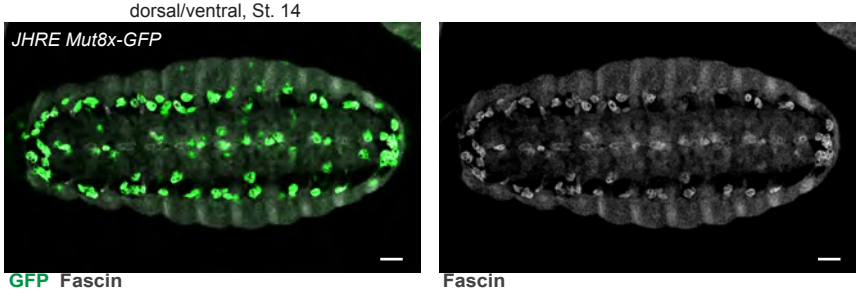

c

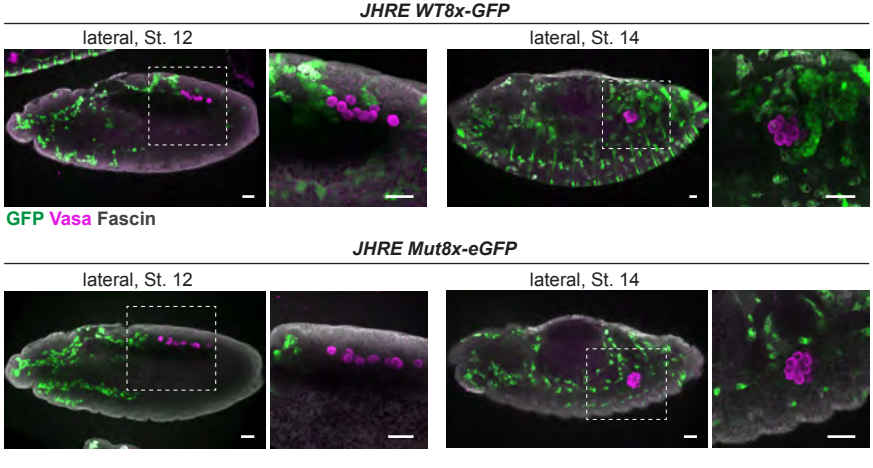

Supplementary Figure 2

Deletions in *jhamt* caused by guide: `CCTGGA|TGTGGTTCAGGATCT`

Class I: frameshift leading to premature stop codon at a.a. 46

Lines with 5 bp deletion to generate `TC|TGT`: 12F1, 12F2

Class II: frameshift leading to premature stop codon at a.a. 54

Lines with `T` deletion to generate `GGA|GT`: 1F1, 1F2, 4F3, 6F2, 6F3, 7F2, 7F3, 8F1, 8F2, 12F3

Lines with `A` deletion to generate `GG|TGT`: 14M2, 14M3

Lines with `TCC` insertion and `G` deletion to generate `GGA|TTCCGT`: 4F1

Supplementary Figure 3

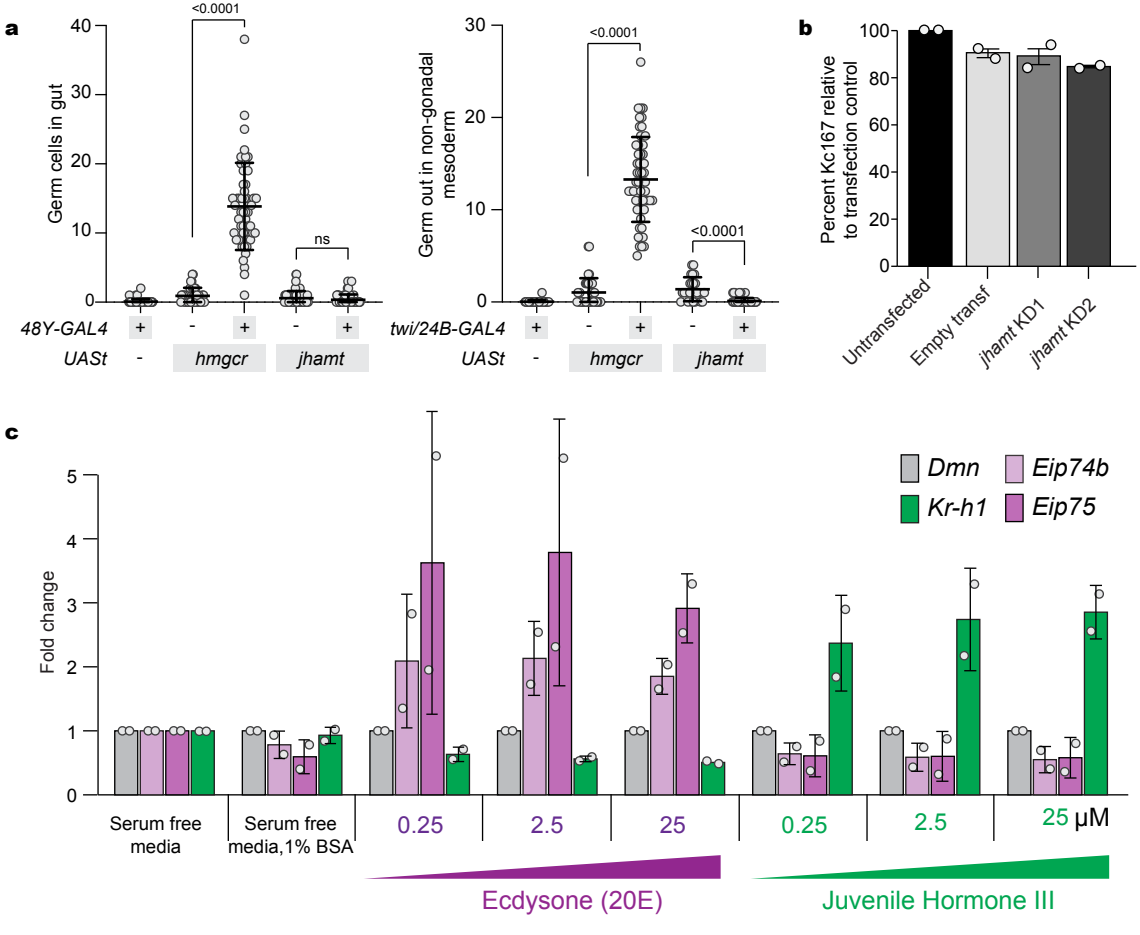

Supplementary Figure 4

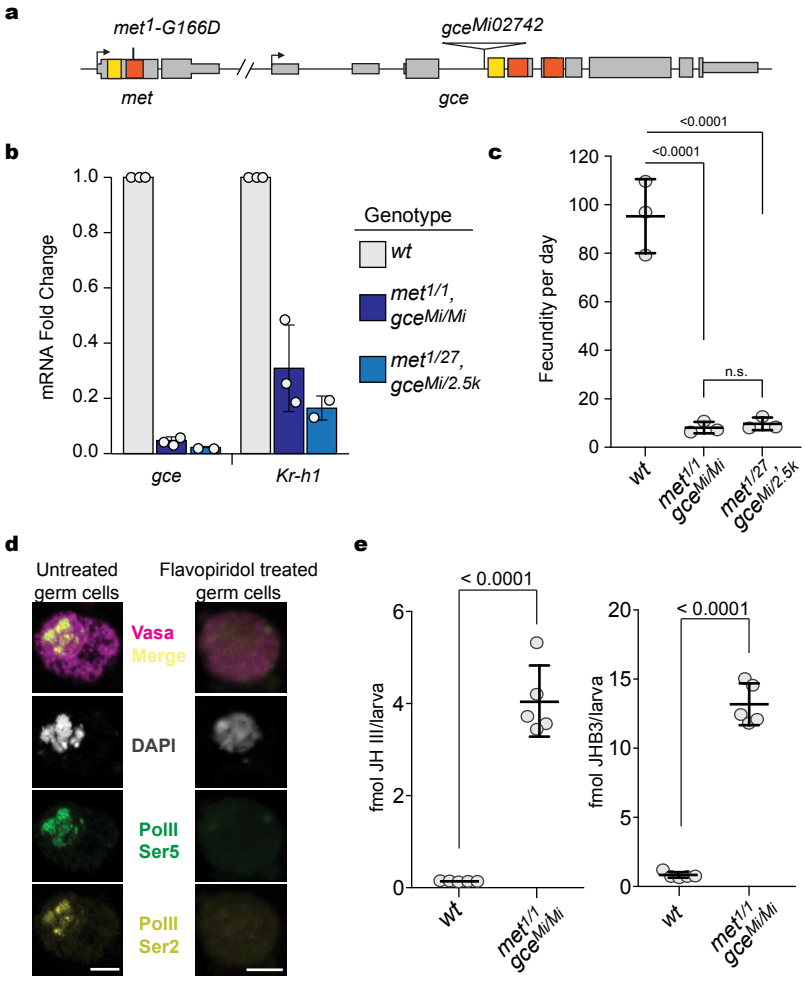
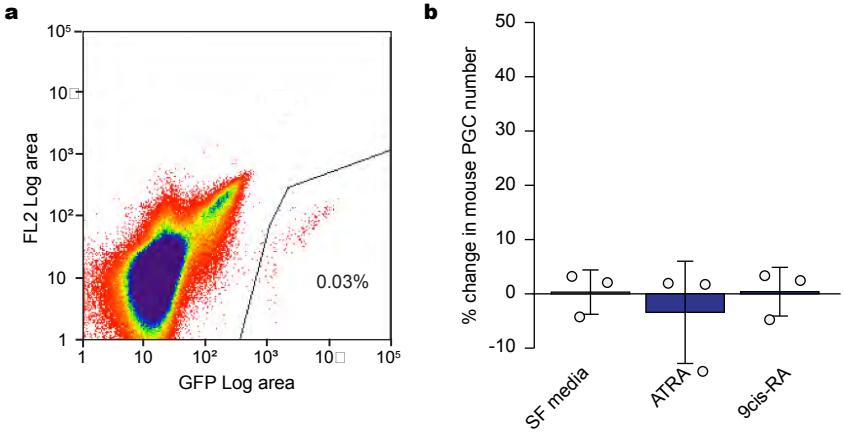
Supplementary Figure 5